Inorg. Chem. **2008**, *47*, 1787−1802

Forum

Water Oxidation by a Ruthenium Complex with Noninnocent Quinone Ligands: Possible Formation of an O−O Bond at a Low Oxidation State of the Metal

James T. Muckerman,*,† Dmitry E. Polyansky,† Tohru Wada,‡ Koji Tanaka,‡ and Etsuko Fujita*,†

Chemistry Department, Brookhaven National Laboratory, Upton, New York 11973-5000, and Coordination Chemistry Laboratories, Institute for Molecular Science, 5-1 Higashiyama, Myodaiji, Okazaki, Aichi 444-8787, Japan

Received September 24, 2007

Tanaka and co-workers reported a novel dinuclear Ru complex, $[Ru_2(OH)_2(3,6\text{-}Bu_2Q)_2(btpyan)](SbF_6)_2$ (3,6-Bu_2Q = 3,6-di*tert*-butyl-1,2-benzoquinone, btpyan = 1,8-bis(2,2′:6′,2″-terpyrid-4′-yl)anthracene), that contains redox active quinone ligands and has an excellent electrocatalytic activity for water oxidation when immobilized on an indium-tin-oxide electrode (*Inorg. Chem.*, **2001**, *40*, 329–337). The novel features of the dinuclear and related mononuclear Ru species with quinone ligands, and comparison of their properties to those of the Ru analogues with the bpy ligand (bpy = 2,2′-bipyridine) replacing quinone, are summarized here together with new theoretical and experimental results that show striking features for both the dinuclear and mononuclear species. The identity and oxidation state of key mononuclear species, including the previously reported oxyl radical, have been reassigned. Our gas-phase theoretical calculations indicate that the Tanaka Ru-dinuclear catalyst seems to maintain predominantly Ru(II) centers while the quinone ligands and water moiety are involved in redox reactions throughout the entire catalytic cycle for water oxidation. Our theoretical study identifies $[Ru_2(O_2^{-})(Q^{-1.5})_2(btpyan)]^0$ as a key intermediate and the most reduced catalyst species that is formed by removal of all four protons before four-electron oxidation takes place. While our study toward understanding the complicated electronic and geometric structures of possible intermediates in the catalytic cycle is still in progress, the current status and new directions for kinetic and mechanistic investigations, and key issues and challenges in water oxidation with the Tanaka catalyst (and its analogues with Cl- or NO_2-substituted quinones and a species with a xanthene bridge instead an antheracene) are discussed.

Introduction

With increasing social and environmental concerns about the twin problems of depletion of fossil fuels and global warming, many researchers consider solar generation of hydrogen from water as the best solution. Yet sunlight-driven water splitting remains a formidable problem. The energetic requirements for water decomposition into H_2 and O_2 (at pH = 7 vs NHE) depend on the number of electrons in the redox half-reactions as shown below.

$$H^+ + e^- \rightarrow H^\bullet \quad E^\circ = -2.61\ \text{V} \tag{1}$$

$$2OH^\bullet + 2H^+ + 2e^- \rightarrow 2H_2O \quad E^\circ = 2.31\ \text{V} \tag{2}$$

$$2H^+ + 2e^- \rightarrow H_2 \quad E^\circ = -0.41\ \text{V} \tag{3}$$

$$O_2 + 4H^+ + 4e^- \rightarrow 2H_2O \quad E^\circ = 0.82\ \text{V} \tag{4}$$

$$H_2O_2 + 2H^+ + 2e^- \rightarrow 2H_2O \quad E^\circ = 1.35\ \text{V} \tag{5}$$

While one-electron reduction and oxidation of water take place at very negative and positive potentials, respectively, the coupled multielectron and multiproton reactions occur at relatively modest potentials (eqs 1–5). Cyanobacteria, algae, and green plants convert solar irradiation into chemical

* To whom correspondence should be addressed. E-mail: muckerma@bnl.gov (J.T.M.), fujita@bnl.gov (E.F.).
† Brookhaven National Laboratory.
‡ Institute for Molecular Science.

10.1021/ic701892v CCC: $40.75
Published on Web 03/10/2008

energy by reducing CO_2 to carbohydrates and oxidizing water to O_2. While nature can carry out photoinduced oxidation and reduction reactions in continuously regenerating and elegant ways, man-made systems have limitations.[1] Metal-oxide-type wide-band-gap semiconductors (i.e., TiO_2, $SrTiO_3$, $NaTaO_3$, their metal-doped/modified materials, etc.), which absorb only 3−5% of solar irradiation, have been successfully used since 1972[2] to split water into H_2 and O_2 under ultraviolet (UV) irradiation.[2–4] These semiconductor materials can support highly energetic one-electron water oxidation (eq 2), but a modest applied potential and/or a metal catalyst such as Pt are frequently needed to promote proton reduction to H_2.[3,5–7] However, this route is closed to narrower-band-gap semiconductors that absorb in the visible. Water oxidation must rely on the four-electron oxidation of water (eq 4), and that generally requires a special catalyst. So far, only a few semiconductor materials that absorb visible light can split water directly upon illumination with the aid of metal catalysts.[8–11] The platinum group metals (Ru, Ir, Pt, Os) have been studied as water oxidation catalysts, and with some optimization an O_2 evolution rate of 40 molecules s^{-1} per surface Ir atom has been achieved with colloidal $IrO_x \cdot nH_2O$[12] using a sacrificial oxidant such as $Ru(bpy)_3^{3+}$. However, the Mn_3CaO_4 cluster at the oxygen-evolving complex (OEC) in photosystem II is capable of turning over about 1000 O_2 molecules s^{-1}.[13] While many binuclear transition-metal catalysts such as $L(H_2O)M-O-M(OH_2)L$ or $L(H_2O)M(BL)-M(OH_2)L$ (where L and BL are nonbridging and bridging organic ligands, respectively) were prepared and characterized for their catalytic properties toward water oxidation,[14–55] none of these molecular catalysts can evolve O_2 faster than one O_2 molecule s^{-1} per catalyst molecule.[16,18,20,38,47,48] Meanwhile, by combining structural and kinetic studies, impressive progress has been achieved in unraveling the molecular mechanism of the catalytic action of the so-called blue dimer,[18–20,22,23,48–55] $[cis,cis\text{-}(bpy)_2(H_2O)Ru-O-Ru(OH_2)(bpy)_2]^{4+}$ (bpy = 2,2′-bipyridine), however, the detailed mechanism of the final stage of the O−O bond formation and O_2 evolution remains unclear.

Recently, Tanaka and co-workers have reported water oxidation catalytic activity of a novel dinuclear Ru complex, $[Ru_2(OH)_2(3,6\text{-}Bu_2Q)_2(btpyan)](SbF_6)_2$ [3,6-Bu_2Q = 3,6-di*tert*-butyl-1,2-benzoquinone; btpyan = 1,8-bis(2,2′:6′,2″-terpyrid-4′-yl)anthracene], that, unlike all other catalytic dinuclear species, contains redox-active quinone ligands.[16] As shown in the top two drawings in Scheme 1, two

(1) McEvoy, J. P.; Brudvig, G. W. *Chem. Rev.* **2006**, *106*, 4455–4483.
(2) Fujishima, A.; Honda, K. *Nature* **1972**, *238*, 37.
(3) Kudo, A.; Kato, H.; Tsuji, I. *Chem. Lett.* **2004**, *33*, 1534–1539.
(4) Wrighton, M. S.; Wolczanski, P. T.; Ellis, A. B. *J. Solid State Chem.* **1977**, *22*, 17–29.
(5) Wrighton, M. S.; Ellis, A. B.; Wolczanski, P. T.; Morse, D. L.; Abrahamson, H. B.; Ginley, D. S. *J. Am. Chem. Soc.* **1976**, *98*, 2774–2779.
(6) Linsebigler, A. L.; Lu, G. Q.; Yates, J. T. *Chem. Rev.* **1995**, *95*, 735–758.
(7) Mills, A.; Le Hunte, S. *J. Photochem. Photobiol. A: Chem.* **1997**, *108*, 1–35.
(8) Maeda, K.; Takata, T.; Hara, M.; Saito, N.; Inoue, Y.; Kobayashi, H.; Domen, K. *J. Am. Chem. Soc.* **2005**, *127*, 8286–8287.
(9) Maeda, K.; Teramura, K.; Lu, D. L.; Takata, T.; Saito, N.; Inoue, Y.; Domen, K. *Nature* **2006**, *440*, 295–295.
(10) Sun, X.; Maeda, K.; Le Faucheur, M.; Teramura, K.; Domen, K. *Appl. Catal. A* **2007**, *327*, 114–121.
(11) Khaselev, O.; Turner, J. A. *Science* **1998**, *280*, 425–427.
(12) Morris, N. D.; Suzuki, M.; Mallouk, T. E. *J. Phys. Chem. A* **2004**, *108*, 9115–9119.
(13) Ruttinger, W.; Dismukes, G. C. *Chem. Rev.* **1997**, *97*, 1–24.
(14) Meyer, T. J.; Huynh, M. H. V. *Inorg. Chem.* **2003**, *42*, 8140–8160.
(15) Wada, T.; Tsuge, K.; Tanaka, K. *Angew. Chem., Int. Ed.* **2000**, *39*, 1479–1482.
(16) Wada, T.; Tsuge, K.; Tanaka, K. *Inorg. Chem.* **2001**, *40*, 329–337.
(17) Pecoraro, V. L.; Baldwin, M. J.; Gelasco, A. *Chem. Rev.* **1994**, *94*, 807–826.
(18) Chronister, C. W.; Binstead, R. A.; Ni, J. F.; Meyer, T. J. *Inorg. Chem.* **1997**, *36*, 3814–3815.
(19) Lebeau, E. L.; Adeyemi, S. A.; Meyer, T. J. *Inorg. Chem.* **1998**, *37*, 6476–6484.
(20) Binstead, R. A.; Chronister, C. W.; Ni, J. F.; Hartshorn, C. M.; Meyer, T. J. *J. Am. Chem. Soc.* **2000**, *122*, 8464–8473.
(21) Yamada, H.; Hurst, J. K. *J. Am. Chem. Soc.* **2000**, *122*, 5303–5311.
(22) Yamada, H.; Koike, T.; Hurst, J. K. *J. Am. Chem. Soc.* **2001**, *123*, 12775–12780.
(23) Yamada, H.; Siems, W. F.; Koike, T.; Hurst, J. K. *J. Am. Chem. Soc.* **2004**, *126*, 9786–9795.
(24) Limburg, J.; Vrettos, J. S.; Liable-Sands, L. M.; Rheingold, A. L.; Crabtree, R. H.; Brudvig, G. W. *Science* **1999**, *283*, 1524–1527.
(25) Limburg, J.; Brudvig, G. W.; Crabtree, R. H. *J. Am. Chem. Soc.* **1997**, *119*, 2761–2762.
(26) Manchanda, R.; Brudvig, G. W.; Crabtree, R. H. *Coord. Chem. Rev.* **1995**, *144*, 1038.
(27) Chen, H. Y.; Faller, J. W.; Crabtree, R. H.; Brudvig, G. W. *J. Am. Chem. Soc.* **2004**, *126*, 7345–7349.
(28) Limburg, J.; Vrettos, J. S.; Chen, H. Y.; de Paula, J. C.; Crabtree, R. H.; Brudvig, G. W. *J. Am. Chem. Soc.* **2001**, *123*, 423–430.
(29) Limburg, J.; Crabtree, R. H.; Brudvig, G. W. *Inorg. Chim. Acta* **2000**, 301–306.
(30) Tagore, R.; Chen, H. Y.; Zhang, H.; Crabtree, R. H.; Brudvig, G. W. *Inorg. Chim. Acta* **2007**, *360*, 2983–2989.
(31) Tagore, R.; Crabtree, R. H.; Brudvig, G. W. *Inorg. Chem.* **2007**, *46*, 2193–2203.
(32) Chen, H. Y.; Tagore, R.; Olack, G.; Vrettos, J. S.; Weng, T. C.; Penner-Hahn, J.; Crabtree, R. H.; Brudvig, G. W. *Inorg. Chem.* **2007**, *46*, 34–43.
(33) Tagore, R.; Chen, H. Y.; Crabtree, R. H.; Brudvig, G. W. *J. Am. Chem. Soc.* **2006**, *128*, 9457–9465.
(34) Yagi, M.; Wolf, K. V.; Baesjou, P. J.; Bernasek, S. L.; Dismukes, G. C. *Angew. Chem., Int. Ed.* **2001**, *40*, 2925–2928.
(35) Ruettinger, W.; Yagi, M.; Wolf, K.; Bernasek, S.; Dismukes, G. C. *J. Am. Chem. Soc.* **2000**, *122*, 10353–10357.
(36) Wu, J. Z.; De Angelis, F.; Carrell, T. G.; Yap, G. P. A.; Sheats, J. C. R.; Dismukes, G. C. *Inorg. Chem.* **2006**, *45*, 189–195.
(37) Yagi, M.; Takahashi, Y.; Ogino, I.; Kaneko, M. *J. Chem. Soc., Faraday Trans.* **1997**, *93*, 3125–3127.
(38) Nagoshi, K.; Yamashita, S.; Yagi, M.; Kaneko, M. *J. Mol. Cat., A: Chem.* **1999**, *144*, 71–76.
(39) Yagi, M.; Osawa, Y.; Sukegawa, N.; Kaneko, M. *Langmuir* **1999**, *15*, 7406–7408.
(40) Yagi, M.; Narita, K. *J. Am. Chem. Soc.* **2004**, *126*, 8084–8085.
(41) Narita, K.; Kuwabara, T.; Sone, K.; Shimizu, K. I.; Yagi, M. *J. Phys. Chem. B* **2006**, *110*, 23107–23114.
(42) Shimazaki, Y.; Nagano, T.; Takesue, H.; Ye, B. H.; Tani, F.; Naruta, Y. *Angew. Chem., Int. Ed.* **2004**, *43*, 98–100.
(43) Sens, C.; Romero, I.; Rodriguez, M.; Llobet, A.; Parella, T.; Benet-Buchholz, J. *J. Am. Chem. Soc.* **2004**, *126*, 7798–7799.
(44) Collin, J. P.; Sauvage, J. P. *Inorg. Chem.* **1986**, *25*, 135–141.
(45) Zong, R. F.; Wang, D.; Hammitt, R.; Thummel, R. P. *J. Org. Chem.* **2006**, *71*, 167–175.
(46) Zong, R.; Thummel, R. P. *J. Am. Chem. Soc.* **2005**, *127*, 12802–12803.
(47) Yagi, M.; Kaneko, M. *Chem. Rev.* **2001**, *102*, 21–35.
(48) Hurst, J. K. *Coord. Chem. Rev.* **2005**, *249*, 313–328.
(49) Gersten, S. W.; Samuels, G. J.; Meyer, T. J. *J. Am. Chem. Soc.* **1982**, *104*, 4029–4030.
(50) Gilbert, J. A.; Eggleston, D. S.; Murphy, W. R.; Geselowitz, D. A.; Gersten, S. W.; Hodgson, D. J.; Meyer, T. J. *J. Am. Chem. Soc.* **1985**, *107*, 3855–3864.
(51) Geselowitz, D.; Meyer, T. J. *Inorg. Chem.* **1990**, *29*, 3894–3896.
(52) Schoonover, J. R.; Ni, J. F.; Roecker, L.; Whiter, P. S.; Meyer, T. J. *Inorg. Chem.* **1996**, *35*, 5885–5892.
(53) Yang, X. F.; Baik, M. H. *J. Am. Chem. Soc.* **2004**, *126*, 13222–13223.
(54) Yang, X.; Baik, M. H. *J. Am. Chem. Soc.* **2006**, *128*, 7476–7485.
(55) Batista, E. R.; Martin, R. L. *J. Am. Chem. Soc.* **2007**, *129*, 7224–7225.

Scheme 1

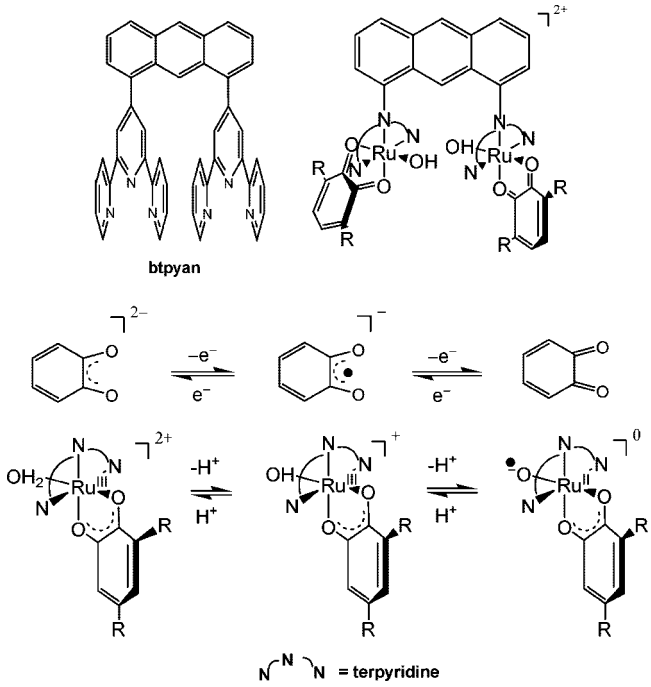

$[Ru(OH)(3,6\text{-}Bu_2Q)]^+$ units are complexed by an anthracene-bridged bis-terpyridine ligand (btpyan) with a geometry in which the two OH groups on the Ru centers are in close proximity for making an O−O bond. The quinone ligand is generally believed to be an electrochemically noninnocent ligand and takes on three different redox states classified as quinone (Q), semiquinone (SQ), and catecholate (Cat), as shown in the second row of Scheme 1. For the dinuclear Ru-quinone complex with an anthracene bridge, the O_2 evolution turnover number (TN) was reported to be 33 500 per catalyst molecule in 40 h for electrolysis carried out in water (pH = 4.0) with the complex deposited on the surface of an indium−tin oxide (ITO) electrode.[16,56] This catalyst is apparently more rapid and more stable than other molecular ruthenium catalysts that have been studied.[16,18,20,38,47,48] Furthermore, the participation of ligand-centered radicals in the interim storage of oxidizing equivalents in the oxidation of coordinated water is a very intriguing feature analogous to that of the OEC. There a tyrosine radical is believed to play a role in electron transfer from the OEC that is coupled with proton transfer from a nearby histidine.[57]

Tanaka and his group further discovered that introduction of the quinone ligand as an electron acceptor into mononuclear aqua-Ru complexes resulted in the formation of $[Ru^{III}(H_2O)(3,5\text{-}Bu_2SQ)(tpy)]^{2+}$ (3,5-Bu_2SQ = 3,5-di-*tert*-butyl-1,2-benzosemiquinone; tpy = 2,2′:6′,2″-terpyridine). Double deprotonation of the aqua ligand without using oxidants produced a new type of complex with an oxyl radical, $[Ru^{II}(O^{\bullet-})(3,5\text{-}Bu_2SQ)(tpy)]$ (see the third row in Scheme 1).[58] It should be noted that these assignments of oxidation states of the metal were based on Ru $3d_{5/2}$ X-ray photoelectron spectra, not their electronic spectra. Are these assignments correct? We will explore this question. The most intriguing structural feature of $[Ru^{II}(O^{\bullet-})(3,5\text{-}Bu_2SQ)(tpy)]$ is a long Ru−O bond length [2.042(6) Å], corresponding to a single bond length.[58] Can we predict such a long Ru−O bond length for the oxyl radical with theoretical calculations?

Although there still exist some inconsistent results and mechanistic questions, in this Article we will summarize the previously published novel features of their mononuclear and dinuclear Ru species with quinone ligands, compare their properties to those of the Ru analogues with the bpy ligand replacing quinone, present new theoretical and experimental results toward understanding the complicated electronic and geometric structures, and discuss new directions for kinetic and mechanistic investigations with the dinuclear analogues to address key issues and challenges in water oxidation. While two types of quinones (i.e., 3,6-Bu_2Q on the Ru dinuclear species and 3,5-Bu_2Q on the Ru mononuclear species) were used in the previous work, we will henceforth simply denote both cases as Q unless otherwise specified. Furthermore, we will remove tpy and btpyan from the mononuclear and dinuclear chemical formulas for simplicity unless it is necessary to describe the nature of the complex being discussed.

The aim of our computational studies has been to guide our experimental mechanistic investigations, making the initial iteration to explain what has been observed and to suggest ideas for future experimental studies. Our initial focus has been on identifying likely reaction intermediates along the catalytic pathway for water oxidation with Tanaka's $[Ru_2(OH)_2(Q)_2(btpyan)]^{2+}$ catalyst complex. This has required the geometry optimization of a large number of species with different compositions, charges, and spin multiplicities. Because the catalyst appears to be quite stable, it is unlikely that an indiscriminately reactive, unstable species (which would degrade the catalyst) is involved in the mechanism. This consideration has allowed us tentatively to reject several possible pathways and to identify what appears to be the most likely one. Our calculations have also aided us in assigning the identity and oxidation states of several species for which such an assignment was ambiguous. In particular, the calculation of UV–vis spectra for comparison with experimental spectra has proved quite useful. We have based the assignments of atomic charge mostly on spin density,[59] which has a well-defined meaning in spin-restricted systems (with eigenfunctions of S^2 and S_z) but not in spin-unrestricted systems (with eigenfunctions only of S_z). Spin contamination in open-shell density functional theory (DFT) calculations and multiconfigurational effects in CASSCF calculations complicated many of the assignments, leading to intermediate cases. Therefore, the assigned fractional atomic and ligand charges in many cases do not comply with conventional integer charges. While our conclusions are still

(56) The TN and current efficiency were mistakenly calculated using 22.4 L for 1 mol of O_2 at room temperature. The correct values are ~10% smaller than the values reported.
(57) Tommos, C.; Babcock, G. T. *Acc. Chem. Res.* **1998**, *31*, 18–25.
(58) Kobayashi, K.; Ohtsu, H.; Wada, T.; Kato, T.; Tanaka, K. *J. Am. Chem. Soc.* **2003**, *125*, 6729–6739.
(59) Remenyi, C.; Kaupp, M. *J. Am. Chem. Soc.* **2005**, *127*, 11399–11413.

evolving, we believe it is important to present a summary and current status of Tanaka's $[Ru_2(OH)_2(Q)_2(btpyan)]^{2+}$ catalyst complex and its related mononuclear species because of their intriguing electronic structures and the uniqueness and effectiveness of the dinuclear species as a water oxidation catalyst.

Experimental Section

Materials. The complex $[Ru^{II}(OH_2)(Q)(tpy)](ClO_4)_2$ (i.e., $[Ru(OH_2)(Q)]^{2+}$) was prepared as previously described for $[Ru^{III}(OH_2)(SQ)(tpy)](ClO_4)_2$ and characterized by NMR, UV–vis, and IR spectroscopy.[58] Tanaka and his group originally assigned this complex as $[Ru^{III}(OH_2)(SQ)]^{2+}$ based on the XPS data,[58] but we now believe this should be assigned as $[Ru^{II}(OH_2)(Q)]^{2+}$ (see Results and Discussion section). We will henceforth denote all species with these new assignments unless otherwise specified.

Instrumental Measurements. UV–vis spectra were measured on a Hewlett-Packard 8452A diode array spectrophotometer and a Cary 500 Scan UV–vis−NIR spectrophotometer. Square-wave voltammograms were obtained using a BAS100 electrochemical system. Measurements were carried out using only one direction (from the rest potential to positive or negative voltage) in an Ar-filled glovebox. The solutions used for the $[Ru(OH_2)(Q)]^{2+}$ experiments contained trifluoroethanol (1–2% by volume) to increase the solubility of $[Ru(OH_2)(Q)]^{2+}$. Between pH = 3 and 10, solutions containing 0.01 M phosphate buffer and 0.1 M sodium triflate were used. Between pH = 1 and 3, solutions containing 0.1 M triflic acid were used after adjustment of the pH with NaOH. Between pH = 10 and 12, solutions containing 0.1 M sodium triflate are used also after adjustment of the pH with NaOH. Glassy C, Pt wire, and Ag/AgCl were used as working, counter, and reference electrodes, respectively, in a one-compartment cell. The surface of the working electrode was cleaned by polishing with alumina after each run.

Water oxidation was conducted by adding a known amount of an acidic $[Ru^{III}(bpy)_3]^{3+}$ or Ce^{IV} solution to a solution containing $[Ru(OH_2)(Q)]^{2+}$. Gaseous products were analyzed by mass spectrometry.

Calculations. All calculations were carried out with the *Gaussian 03* program package[60] using the LANL2DZ ECP basis[61–63] for Ru and the D95V basis[64] for all other elements. This is referred to in Gaussian as the LANL2DZ basis. Most calculations employed the hybrid DFT B3LYP method,[65–67] but these were complemented by selected CAS(4,4) calculations.[68–73] Time-dependent B3LYP (TD-B3LYP) calculations were carried out with the *Gaussian 03* program to predict UV–vis spectra of various species. Because the focus of the calculations presented here is to elucidate the properties of a large number of possible intermediate species along the reaction pathway and not on the detailed energetics and kinetics of the catalytic reaction, we have employed this relatively small basis and have neglected the effects of solvation, counterions, and interactions with explicit solvent molecules. We have further taken the expediency of substituting H for *t*-Bu on the quinone ligands of the dinuclear spcies (but not the mononuclear species).

Results and Discussion

Spectroscopic and Electrochemical Properties of Mononuclear Species. Tanaka and co-workers[58] proposed that the ruthenium oxyl radical complex $[Ru^{II}(O^{\bullet-})(SQ)]^0$ was prepared by the double deprotonation of the aqua ligand of $[Ru^{III}(OH_2)(SQ)]^{2+}$ through $[Ru^{III}(OH)(SQ)]^+$ as shown in eq 6.

$$[Ru^{III}(OH_2)(SQ)]^{2+} \underset{+H^+}{\overset{-H^+}{\rightleftharpoons}} [Ru^{III}(OH)(SQ)]^{+} \underset{+H^+}{\overset{-H^+}{\rightleftharpoons}} [Ru^{II}(O^{\bullet-})(SQ)] \quad (6)$$

The assignment of the oxidation state of Ru and the quinone ligand is subject to disagreement for the aqua and hydroxyl species. In fact, in many cases, the assignment of oxidation states of Ru (and Os) complexes containing a quinone ligand has been ambiguous even using data such as X-ray structures, UV–vis, X-ray photoelectron, and EPR spectra.[74–83] Even a detailed analysis of DFT-calculated structures, spin densities, and **g**-tensor anisotropies led to ambiguous (i.e., intermediate) assignments for a series of $[Ru(Q)(acac)_2]^{-,0,+}$ complexes with different Q. The formal metal oxidation state of Ru was best described as being intermediate between Ru^{II} and Ru^{III} and only predominantly Ru^{III} in the electron-deficient cationic complexes.[59] In a series of Ru systems with neutral diimine-type coligands, Lever and co-workers[83] found that a Ru^{II} assignment provided the best overall description of all of the catecholate, semiquinone, and quinone complexes they studied. To avoid any confusion, we first state our current assignments for the reactions (see eq 7) and use our assignment if appropriate.

$$[Ru^{II}(OH_2)(Q)]^{2+} \underset{+H^+}{\overset{-H^+}{\rightleftharpoons}} [Ru^{II}(OH)(Q)]^{+} \underset{+H^+}{\overset{-H^+}{\rightleftharpoons}} [Ru^{II}(O^{\bullet-})(SQ)] \xrightarrow{H^{\bullet}} [Ru^{II}(OH)(SQ)] \quad (7)$$

The $[Ru^{II}(OH_2)(Q)]^{2+}$ complex has a strong metal-to-quinone charge-transfer band at 600 nm in acidic aqueous

(60) Frisch, M. J.; et al. *Gaussian 03*, revision B.04; Gaussian, Inc.: Wallingford, CT, 2004.
(61) Hay, P. J.; Wadt, W. R. *J. Chem. Phys.* **1985**, *82*, 270–283.
(62) Hay, P. J.; Wadt, W. R. *J. Chem. Phys.* **1985**, *82*, 299–310.
(63) Wadt, W. R.; Hay, P. J. *J. Chem. Phys.* **1985**, *82*, 284–298.
(64) Dunning, T. H. J.; Hay, P. J. *Modern Theoretical Chemistry*; Plenum: New York, 1976.
(65) Becke, A. D. *Phys. Rev. A* **1988**, *38*, 3098–3100.
(66) Lee, C.; Yang, W.; Parr, R. G. *Phys. Rev. B* **1988**, *37*, 785–789.
(67) Miehlich, B.; Savin, A.; Stoll, H.; Preuss, H. *Chem. Phys. Lett.* **1989**, *157*, 200–206.
(68) Hegarty, D.; Robb, M. A. *Mol. Phys.* **1979**, *38*, 1795.
(69) Eade, R. H. E.; Robb, M. A. *Chem. Phys. Lett.* **1981**, *83*, 362.
(70) Schlegel, H. B.; Robb, M. A. *Chem. Phys. Lett.* **1982**, *93*, 43.
(71) Bernardi, F.; Bottini, A.; McDougall, J. J. W.; Robb, M. A.; Schlegel, H. B. *Faraday Symp. Chem. Soc.* **1984**, *19*, 137.
(72) Yamamoto, N.; Vreven, T.; Robb, M. A.; Frisch, M. J.; Schlegel, H. B. *Chem. Phys. Lett.* **1996**, *250*, 373.
(73) Frisch, M. J.; Ragazos, I. N.; Robb, M. A.; Schlegel, H. B. *Chem. Phys. Lett.* **1992**, *189*, 52.
(74) Haga, M.; Isobe, K.; Boone, S. R.; Pierpont, C. G. *Inorg. Chem.* **1990**, *29*, 3795–3799.
(75) Pierpont, C. G.; Buchanan, R. M. *Coord. Chem. Rev.* **1981**, *38*, 45–87.
(76) Pierpont, C. G.; Lange, C. W. In *Progress Inorganic Chemistry*; Karlin, K., Ed.; Wiley: New York, 1993; Vol. *41*.
(77) Auburn, P. R.; Dodsworth, E. S.; Haga, M.; Liu, W.; Nevin, W. A.; Lever, A. B. P. *Inorg. Chem.* **1991**, *30*, 3502–3512.
(78) Lever, A. B. P.; Auburn, P. R.; Dodsworth, E. S.; Haga, M.; Wei, L.; Melnik, M.; Nevin, W. A. *J. Am. Chem. Soc.* **1988**, *110*, 8076–8084.
(79) Haga, M.; Dodsworth, E. S.; Lever, A. B. P.; Boone, S. R.; Pierpont, C. G. *J. Am. Chem. Soc.* **1986**, *108*, 7413–7414.
(80) Haga, M.; Dodsworth, E. S.; Lever, A. B. P. *Inorg. Chem.* **1986**, *25*, 447–453.

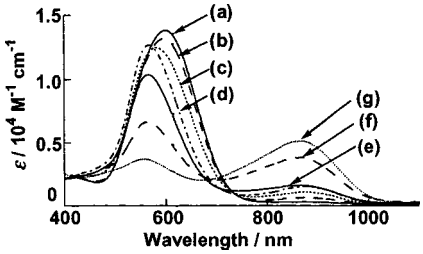

Figure 1. pH-dependent UV–vis spectra of $[Ru(OH_2)(Q)]^{2+}$: (a) pH = 3.2, (b) pH = 4.5, (c) pH = 5.6, (d) pH = 7.1, (e) pH = 10.1, (f) pH = 11, and (g) pH = 12.0. Reprinted with permission from ref 58. Copyright 2003 American Chemical Society.

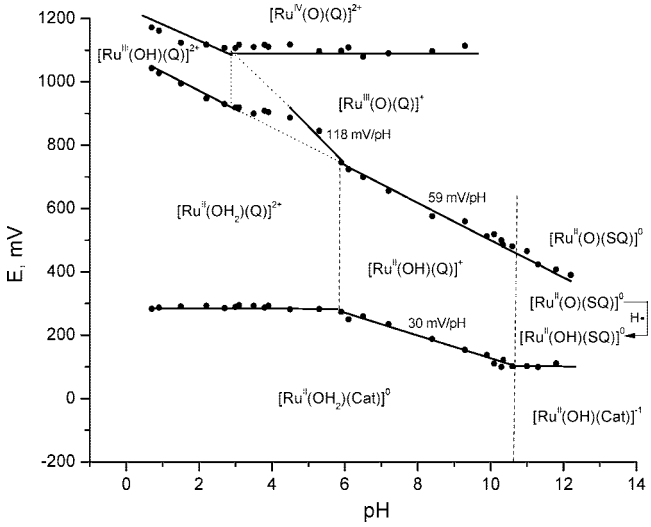

Figure 2. Plots of $E_{1/2}$ (V vs Ag/AgCl) vs pH for $[Ru(OH_2)(Q)(tpy)]^{2+}$ in aqueous solution containing 1–2% CF_3CH_2OH.

solutions (Figure 1).[58] The addition of a base shifted the band maximum to 576 nm, and the absorbance at 576 nm reached a maximum at pH = 7.1. Further addition of a base resulted in the appearance of another band at 870 nm with a concomitant decrease in the intensity of the 576 nm band. From the spectroscopic method, the pK_a's of $[Ru^{II}(OH_2)(Q)]^{2+}$ and $[Ru^{II}(OH)(Q)]^{+}$ are determined to be 5.5 and 10.7, respectively.[58]

In order to characterize the redox properties of $[Ru^{II}(OH_2)(Q)]^{2+}$, we have measured cyclic voltammograms (CVs) at various pH values (Figure 2). Unfortunately, the species formed above pH = 10, previously assigned as $[Ru^{II}(O^{\bullet-})(SQ)]^0$, precipitates; therefore, trifluoroethanol (1–2% by volume) was added to the aqueous solution. In a Pourbaix diagram, crossing a line in moving from bottom to top represents the oxidation of the metal center or the oxidation of semiquinone (or catecholate). From left to right on the diagram, crossing a vertical line represents the removal of a proton from the species at the left of the line. We use the pK_a values previously determined by base titration (5.5 and 10.7) for $[Ru^{II}(OH_2)(Q)]^{2+}$ and $[Ru^{II}(OH)(Q)]^{+}$, respectively, to draw lines in the Pourbaix diagram. While a diagonal line of 59 mV/pH represents the removal of a proton coupled to the removal of an electron, diagonal lines of 30

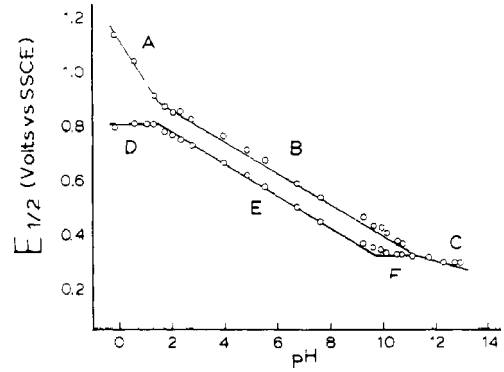

Figure 3. Plots of $E_{1/2}$ (V vs SSCE) vs pH for $[Ru(OH_2)(bpy)(tpy)]^{2+}$ in aqueous solution: (A) $Ru^{IV}O^{2+}/Ru^{III}OH_2^{3+}$; (B) $Ru^{IV}O^{2+}/Ru^{III}OH^{2+}$; (C) $Ru^{IV}O^{2+}/Ru^{II}OH^{+}$; (D) $Ru^{III}OH_2^{3+}/Ru^{II}OH_2^{2+}$; (E) $Ru^{III}OH^{2+}/Ru^{II}OH_2^{2+}$; (F) $Ru^{III}OH^{2+}/Ru^{II}OH^{+}$. Reprinted with permission from ref 84. Copyright 1984 American Chemical Society.

and 118 mV/pH indicate two electrons coupled with one proton and one electron coupled with two protons, respectively. Interestingly, the Pourbaix diagram shows a diagonal line (59 mV/pH) above pH = 10.5, inconsistent with the formation of $[Ru^{II}(O^{\bullet-})(SQ)]^0$. Because $[Ru^{II}(O^{\bullet-})(SQ)]^0$ is a very reactive oxyl radical, it may abstract an H atom from CF_3CH_2OH to form $[Ru^{II}(OH)(SQ)]^0$. We will discuss more about $[Ru^{II}(O^{\bullet-})(SQ)]^0$ vs $[Ru^{II}(OH)(SQ)]^0$ in the Electronic Structure Calculations section. Another intriguing process that involves two electrons and one proton is observed between pH = 5.5 and 10.5 to yield $[Ru^{II}(OH_2)(Cat)]^0$ from $[Ru^{II}(OH)(Q)]^{+}$. While observed currents in square-wave voltammograms implicate the involvement of two-electron processes in water (pH = 1−10), consecutive one-electron processes for Q/SQ and SQ/Cat are observed in CH_2Cl_2.[58] Furthermore, the oxidation of $[Ru^{II}(OH_2)(Q)]^{2+}$ between pH = 3 and 6 appears to involve quite complicated processes. We are currently using pulse radiolysis and spectroelectrochemistry to identify the intermediate species involved in the redox chemistry.

The bpy analogue, $[Ru^{II}(OH_2)(bpy)(tpy)]^{2+}$, of $[Ru^{II}(OH_2)(Q)(tpy)]^{2+}$ (or $[Ru^{II}(OH_2)(Q)]^{2+}$) has been investigated by Takeuchi et al.,[84] and the results are shown in Figure 3 for comparison with $[Ru^{II}(OH_2)(Q)]^{2+}$. As can be seen from the figure, the pK_a of $[Ru^{II}(OH_2)(bpy)]^{2+}$ is about 10, which is much larger than that of $[Ru^{II}(OH_2)(Q)]^{2+}$ (pK_a = 5.5). While the proton-coupled oxidation to form $[Ru^{IV}(O)(bpy)]^{2+}$ (eq 8) can be accomplished by applying potentials smaller than 0.8 V between pH = 3 and 10 (Figure 2), the formation of $[Ru^{IV}(O)(Q)]^{2+}$ from $[Ru^{III}(O)(Q)]^{2+}$ is not coupled to a proton transfer and requires a more positive potential (1.1 V).

$$[Ru^{II}(OH_2)(bpy)]^{2+} \underset{-H^+,\,+e^-}{\overset{-H^+,\,-e^-}{\rightleftharpoons}} [Ru^{III}(OH)(bpy)]^{2+} \underset{-H^+,\,+e^-}{\overset{-H^+,\,-e^-}{\rightleftharpoons}} [Ru^{IV}(O)(bpy)]^{2+} \quad (8)$$

Because mononuclear Ru complexes prepared by Thummel and his group show catalytic activity for water oxidation using Ce^{IV}/H^+,[46] we tested to determine if $[Ru^{II}(OH_2)(Q)]^{2+}$

(81) Bhattacharya, S.; Boone, S. R.; Fox, G. A.; Pierpont, C. G. *J. Am. Chem. Soc.* **1990**, *112*, 1088–1096.
(82) Bhattacharya, S.; Pierpont, C. G. *Inorg. Chem.* **1992**, *31*, 35–39.
(83) Masui, H.; Lever, A. B. P.; Auburn, P. A. *Inorg. Chem.* **1991**, *30*, 2402–2410.
(84) Takeuchi, K. J.; Thompson, M. S.; Pipes, D. W.; Meyer, T. J. *Inorg. Chem.* **1984**, *23*, 1845–1851.

acts as a catalyst (or a catalyst precursor) using Ce^{IV}/H^+ (pH = 1) and also $Ru(bpy)_3^{3+}/H^+$ (pH = 1) as the oxidant. We did not detect any O_2 formation in either case by mass spectrometry.

Now the assignment of the oxidation state of Ru and the quinone ligand of $[Ru^{II}(OH_2)(Q)]^{2+}$ and $[Ru^{II}(OH)(Q)]^+$ will be discussed. The assignments of related quinone complexes have been problematic, and many controversies have been created.[74,77,81,85,86] The rest potentials of $[Ru^{II}(OH_2)(Q)]^{2+}$ and $[Ru^{II}(OH)(Q)]^+$ are 0.48 and 0.36 V, respectively, consistent with the assignment of quinone assuming the Q/SQ reduction potential is 0.31 V.[58] The X-ray single-crystal structures of $[Ru^{II}(OH_2)(Q)]^{2+}$, "$[Ru^{II}(O^{\bullet -})(SQ)]^0$", and $[Ru^{II}(OC(O)CH_3)(SQ)]^0$ have been determined.[58] C−O bond lengths of quinone/semiquinone/catecholate ligands should reflect the charge distribution of the metal 1,2-benzoquinone complexes. The average distances of the two C−O bonds (C1−O and C2−O) are 1.289, 1.35, and 1.326 Å for $[Ru^{II}(OH_2)(Q)]^{2+}$, "$[Ru^{II}(O^{\bullet -})(SQ)]^0$", and $[Ru^{II}(OC(O)CH_3)(SQ)]^0$, respectively. Furthermore, the C4−C5 distances are 1.454, 1.39, and 1.430 Å, respectively. These bond distances imply that the assignment of $[Ru^{II}(OH_2)(Q)]^{2+}$ is correct. The strong charge-transfer bands observed around 600 nm in the spectra of $[Ru^{II}(OH_2)(Q)]^{2+}$ and $[Ru^{II}(OH)(Q)]^+$ also suggest that the quinone ligands have the same redox structure, and the bands observed at 870 nm in the spectra of "$[Ru^{II}(O^{\bullet -})(SQ)]^0$" and $[Ru^{II}(OC(O)CH_3)(SQ)]^0$ are good evidence of the semiquinone structure in these complexes. All of these assignments as Ru^{II} are consistent with the aqua and hydroxyl species having the quinone structures. Additional theoretical support for these assignments will be given below.

Electronic Structure Calculations. While one would expect that the open-shell triplet species ($[Ru^{III}(H_2O)(SQ)]^{2+}$ and $[Ru^{III}(OH)(SQ)]^+$) would be lower in energy than the corresponding open-shell singlet states by $2J$ (where J is the exchange integral involving the two relevant electrons), these species are diamagnetic. This fact prompted Tanaka and coworkers to propose a strong "antiferromagnetic interaction" between the spins on the Ru^{III} and SQ.[58] Our B3LYP/LANL2DZ calculations disagree with Tanaka's assignments: for the aquo species they indicate that the closed-shell singlet $[Ru^{II}(OH_2)(Q)]^{2+}$ is more stable than triplet $[Ru^{III}(OH_2)(SQ)]^{2+}$ by 8.3 kcal/mol and predict a triplet assignment for $[Ru^{III}(OH)(SQ)]^+$, which implies that it should be paramagnetic. However, our CAS(4,4) calculations of the singlet and triplet hydroxo species indicate that the singlet is multiconfigurational (while the triplet is not) and that a generalized valence-bond configuration interaction (CI) between π-bonding and π-antibonding molecular orbitals between the Ru and quinone stabilizes the singlet sufficiently for it to be the ground electronic state. The projection of these 2 × 2 molecular orbital interactions on fragment Ru and quinone orbitals suggests that the ground-state singlet

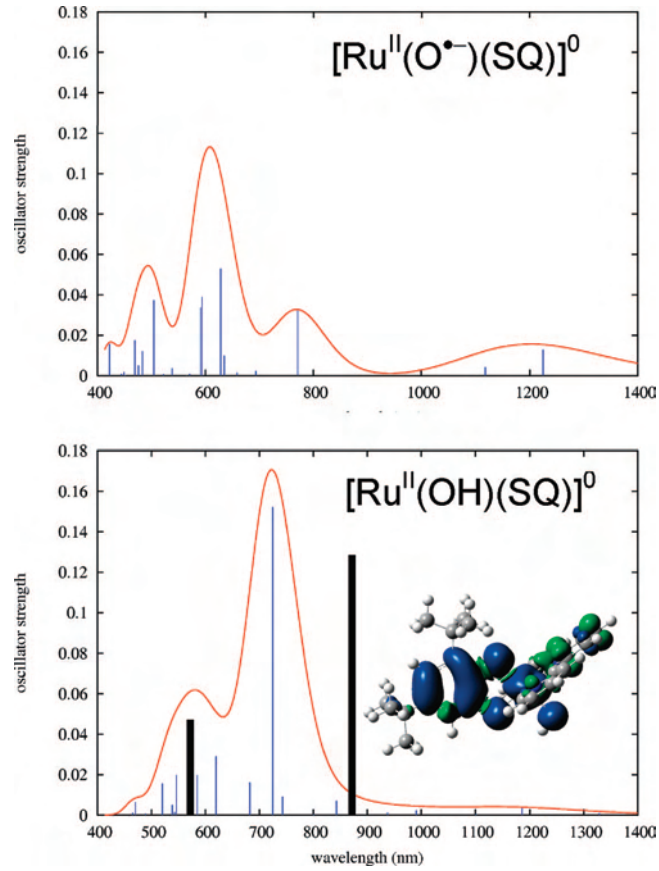

Figure 4. Calculated spectra of $[Ru(O^{\bullet -})(SQ)]^0$ (top) and $[Ru(OH)(SQ)]^0$ (bottom). The vertical lines (blue) are the discrete transitions from a TD-B3LYP/LANL2DZ calculation, and the smooth curves (red) are the result of broadening with a Gaussian function of width 0.18 (top) and 0.10 (bottom) eV. In the bottom panel, the black vertical bars indicate the (unnormalized) peaks of the experimental spectrum and the inset shows the calculated spin density (isovalue = 0.0004). Spin−flip transitions were neglected in these calculations.

should have some open-shell singlet character. TD-B3LYP-calculated $[Ru^{II}(OH_2)(Q)]^{2+}$, $[Ru^{II}(OH)(Q)]^+$ (singlet), and $[Ru^{III}(OH)(SQ)]^+$ (triplet) spectra are shown in Figures S1 and S2 in the Supporting Information. The calculated triplet $[Ru^{III}(OH)(SQ)]^+$ spectrum exhibits a very weak absorption around 700 nm, while both the singlet and triplet absorb strongly around 570 nm.

The strange behavior of $[Ru^{II}(O^{\bullet -})(SQ)]^0$ in the Pourbaix diagram has been discussed in the previous section. As noted above, our experimental and CAS(4,4) results assign the "2+" and "1+" species as $Ru^{II}(Q)$, and we further question the assignment of the Ru-oxyl triplet $[Ru^{II}(O^{\bullet -})(SQ)]^0$ species as the end product. In order to identify the species existing above pH = 10, we have carried out TD-B3LYP calculations for triplet $[Ru^{II}(O^{\bullet -})(SQ)]^0$ (see Figure 4) and have repeated the base titration experiments to measure absorption bands in the NIR region. However, we have not observed a NIR band for $[Ru^{II}(O^{\bullet -})(SQ)]^0$ as predicted by TD-B3LYP. Our TD-B3LYP calculations of the electronic spectra of $Ru^{II}(O^{\bullet -})(SQ)^0$ and $Ru^{II}(OH^{\bullet -})(SQ)^0$ (Figure 4) indicate a much better match between the latter and the observed spectrum (positions and relative intensities of experimental peaks indicated by black bars), indicating that the $Ru^{II}(O^{\bullet -})(SQ)$ species probably abstracts an H atom from

(85) Shepherd, R. E.; Proctor, A.; Henderson, W. W.; Myser, T. K. *Inorg. Chem.* **1987**, *26*, 2440.
(86) Wada, T.; Yamanaka, M.; Fujihara, T.; Miyazato, Y.; Tanaka, K. *Inorg. Chem.* **2006**, *45*, 8887–8894.

Table 1. DFT-Calculated Bond Distances (Å) for Ru Mononuclear Species[a]

	$[Ru^{II}(OH_2)(Q)]^{2+}$ singlet	$[Ru^{II}(OH)(Q)]^{+}$ singlet	$[Ru^{III}(OH)(SQ)]^{+}$ triplet	$[Ru^{II}(O^{\bullet-})(SQ)]^{0}$ triplet	$[Ru^{II}(OH)(SQ)]^{0}$ doublet
Ru−O (H_2O moiety)	2.147 (2.099)	1.977	1.956	1.824 (2.043)	2.018
Ru−O1	2.024 (1.968)	2.022	2.095	2.202 (1.985)	2.064
Ru−O2 (quinone)	2.081 (2.028)	2.103	2.071	2.136 (2.058)	2.095
C1−O1	1.308 (1.293)	1.327	1.346	1.328 (1.35)	1.357
C2−O2 (quinone)	1.312 (1.280)	1.324	1.342	1.329 (1.34)	1.350
C3−C4	1.390 (1.357)	1.391	1.392	1.391 (1.38)	1.399
C5−C6	1.384 (1.365)	1.389	1.397	1.394 (1.39)	1.402
C4−C5 (quinone)	1.472 (1.454)	1.545	1.445	1.443 (1.39)	1.431

[a] Numbers in parentheses indicate bond distances determined X-ray single-crystal diffractions.[58] Here O1 is the quinone oxygen trans to OH_2, OH, or O. Carbon atoms C4 and C6 have *t*-Bu groups in the nomenclature used in this table.

somewhere (possibly such as methanol, trifluoroethanol, or 2-methoxyethanol) to form doublet $Ru^{II}(OH)(SQ)^0$. In fact, our spin-restricted open-shell Hartree–Fock (ROHF) and CAS(4,4) calculations indicate that the principal configuration of triplet $[Ru^{II}(O^{\bullet-})(SQ)]^0$ is actually $[Ru^{III}(O^{\bullet-})(Cat)]^0$ while our spin-unrestricted B3LYP (UB3LYP) calculations have sufficient spin contamination ($S_2 = 2.471$ before annihilation) to be ambiguous on this point. The highest doubly occupied orbital in the ROHF calculation is the catecholate highest occupied molecular orbital (HOMO),[87] and the CAS(4,4) wave function is 100% the ROHF wave function. Atomic spin densities from a spin-restricted open-shell B3LYP (ROB3LYP) calculation at the UB3LYP-optimized geometry predict 0.418 of an electron on Ru, 0.623 of an electron on the oxyl O, and 0.893 of an electron on the quinone ligand, mostly on the two O atoms and the aromatic ring, and the orbital corresponding to the catecholate HOMO is only singly occupied. This is most consistent with the $[Ru^{II}(O^{\bullet-})(SQ)]^0$ assignment. In either case, the calculations predict an oxyl radical species.

The calculated long Ru−O bond distance and the 0.05 Å difference in the various C−C bonds in the quinone ligand for $[Ru^{II}(O^{\bullet-})(SQ)]^0$ imply semiquinone character (see Table 1). Additionally, the B3LYP calculations on the inferred neutral oxyl species suggest that the Ru−O bond distance should be 1.824 Å while the experimental X-ray crystallographic bond length in the isolated species is 2.043 Å. This discrepancy supports our spectroscopic evidence implicating the neutral doublet hydroxo species, for which we calculated a Ru−O bond length of 2.018 Å in much better accord with the experimental result. All other calculated structural features of $[Ru^{II}(OH)(SQ)]^0$ fit well with those of the X-ray structure of "$[Ru^{II}(O^{\bullet-})(SQ)]^0$". It is reported[58] that $[Ru(OH_2)(Q)]^{2+}$ does not show any EPR signals in CH_2Cl_2 at 193 or 3.9 K as expected from its singlet nature. However, at 193 K, a broad isotropic signal at $g = 2.029$ is reported to appear upon the addition of *more* than 1.0 equiv of *t*-BuOK. This indicates that $[Ru(OH)(Q)]^+$ is also a singlet. Interestingly, the intensity of the signal increased with an increase of the amount of *t*-BuOK up to 3.0 equiv. Tanaka and co-workers attributed the triplet signals to $[Ru^{II}(O^{\bullet-})(SQ)]^0$, asserting "The EPR at 3.9 K exhibited an isotropic broad signal with a hyperfine structure at the $\Delta m_s = 1$ region and an isotropic signal at $\Delta m_s = 2$ region, indicating the triplet state of a biradical compound."[58] This EPR signal might be due to the presence of unreacted $[Ru(O^{\bullet-})(SQ)]^0$, because the H atom transfer reaction should be very slow or may not occur at such low temperature.

Acid–Base, Redox, and Catalytic Properties of $[Ru_2(OH)_2(Q)_2(btpyan)](SbF_6)_2$. Wada et al. reported the preparation and catalytic activity of $[Ru_2(OH)_2(Q)_2(btpyan)](SbF_6)_2$ in 2000 and 2001.[15,16] This complex is not soluble in water. The electronic spectrum of this complex in MeOH showed a strong band at 576 nm, which is indicative of a metal-to-quinone charge-transfer band. The gradual addition of 2 equiv of *t*-BuOK to the solution results in the gradual appearance of a new band at 850 nm and the disappearance of the band at 576 nm.[16]

$$[Ru(OH)(Q)Ru(OH)(Q)]^{2+} \underset{2H^+}{\overset{-2H^+}{\rightleftharpoons}} [Ru(O)(SQ)Ru(O)(SQ)]^0 \quad (9)$$

In eq 9, the acid–base equilibrium of the OH group of $[Ru(OH)(Q)Ru(OH)(Q)]^{2+}$ is coupled with the reduction of quinone to semiquinone as found in the case of the mononuclear analogue. Similar pH-dependent spectra are also observed for the species deposited on an ITO electrode in water. The strong metal-to-ligand charge-transfer band at 578 nm in water below pH = 2.0 gradually decreased in intensity above pH = 2.0, and the intensity of a new band at 850 nm increased up to pH = 3.0, indicating that the two pK_a's of $[Ru(OH)(Q)Ru(OH)(Q)]^{2+}$ are between 2.0 and 3.0.[16] However, our DFT calculations indicate that the monodeprotonated species of $[Ru(OH)(Q)Ru(OH)(Q)]^{2+}$ is $[(SQ)Ru(OH\cdots O)Ru(SQ)]^+$ with a hydrogen-bonded ($OH\cdots O$) bridge and semiquinone ligands (see the computational sections), indicating that the second pK_a must be larger than the first one. More detailed experiments are needed to clarify this issue.

The CV of $[Ru(OH)(Q)Ru(OH)(Q)]^{2+}$ in MeOH shows four nearly reversible redox couples at $E_{1/2} = +0.43$, $+0.35$, -0.47, and -0.56 V, which can be assigned to the ligand-localized reductions of two quinones (i.e., two Q/SQ couples and two SQ/Cat couples) on the basis of the rest potential of $[Ru(OH)(Q)Ru(OH)(Q)]^{2+}$ (0.49 V).[16] The addition of 2 equiv of *t*-BuOK shifts the rest potential of the MeOH solution from +0.49 to −0.12 V, consistent with the conversion from $[Ru(OH)(Q)Ru(OH)(Q)]^{2+}$ to $[Ru(O)(SQ)Ru(O)(SQ)]^0$ (eq 9). In addition to two reversible redox couples at $E_{1/2} = 0.40$ and 0.30 V, not-well-defined successive reductions likely associated with the production of $[Ru(O)(SQ)Ru(O)(Cat)]^-$ and $[Ru(O)(Cat)Ru(O)(Cat)]^{2-}$ are observed between −0.43 and −0.68 V.[16]

(87) Tsai, M.-K.; Muckerman, J. T.; Fujita, E., to be published.

Because MeOH undergoes irreversible oxidation at potentials more positive than 1.0 V (vs Ag/AgCl), the CVs of $[Ru(OH)(Q)Ru(OH)(Q)]^{2+}$ were recorded up to 1.8 V in trifluoroethanol/ether (50/50, v/v) to detect the Ru^{II}/Ru^{III} redox couples.[16] An irreversible anodic wave is observed at $E_p = 1.34$ V corresponding to sequential one-electron-oxidation reactions based on the area (i.e., $2e^-$ equivalents) of the broad anodic wave. This process was assigned previously as eq 10 in trifluoroethanol/ether,[16] but the formation of $[Ru^{II}(O)(SQ)Ru^{II}(O)(SQ)]^0$ and its reactions such as eq 11 possibly occur with a trace amount of water in the solution because of the strong acidity of $[Ru^{II}(OH)(Q)Ru^{II}(OH)(Q)]^{2+}$.

$$[Ru^{II}(OH)(Q)Ru^{II}(OH)(Q)]^{2+} \rightarrow [Ru^{III}(OH)(Q)Ru^{II}(OH)(Q)]^{3+} \rightarrow [Ru^{III}(OH)(Q)Ru^{III}(OH)(Q)]^{4+} \quad (10)$$

$$[Ru^{II}(O)(Q)Ru^{II}(O)(Q)]^{2+} \rightarrow [Ru^{III}(O)(Q)Ru^{II}(O)(Q)]^{3+} \rightarrow [Ru^{III}(O)(Q)Ru^{III}(O)(Q)]^{4+} \quad (11)$$

In fact, the addition of water to the solution resulted in a large catalytic current at potentials more positive than 1.0 V. The controlled-potential electrolysis of $[Ru^{II}(OH)(Q)Ru^{II}(OH)(Q)]^{2+}$ in CF_3CH_2OH containing water (10%) at 1.70 V evolved O_2 with a current efficiency of 91% with TN = 21. Under these conditions, the pH was not controlled by a buffer, and the solution became highly acidic after 21 turnovers owing to the production of 84 equiv of protons. Under such an acidic condition, the catalyst may be converted to the diaquo species and oxidized to form the anthracene cation radical. This would lead to the decomposition of the catalyst.

The CV of an ITO electrode modified by $[Ru^{II}(OH)(Q)Ru^{II}(OH)(Q)]^{2+}$ (1.2×10^{-8} mol/2.0 cm^2) in water (pH = 4.0) shows a broad redox wave centered at 0.32 V (vs Ag/AgCl), an irreversible wave at 1.19 V, and a strong catalytic current above 1.5 V.[16] Although an ITO electrode slowly evolved O_2 even in the absence of a catalyst at 1.70 V above pH = 5.0, such water oxidation can be avoided when electrolysis was carried out below pH = 4.0. So far, the pH-dependent CV of the Ru-modified ITO electrode has not determined the details required for construction of a Pourbaix diagram. Controlled-potential electrolysis at pH = 4.0 using an ITO electrode modified by $[Ru^{II}(OH)(Q)Ru^{II}(OH)(Q)]^{2+}$ (2.0×10^{-8} mol/10 cm^2) was reported to produce O_2 with a maximum TN = 33 500 per catalyst molecule in 40 h.[16,56] When an ITO electrode modified by a larger amount of $[Ru^{II}(OH)(Q)Ru^{II}(OH)(Q)]^{2+}$ (1.0×10^{-7} mol/10 cm^2) was prepared, a TN of 6730 was reported.[15,56] The current efficiency for O_2 evolution was 95% and the TN was 500 after 20.2 C had passed in the electrolysis.[15,56] The heterogeneous catalytic activity depends on the amount of the catalyst, the catalyst deposition (i.e., smooth monolayer vs islands), the catalyst purity (i.e., high catalytic currents and TNs require an extremely pure catalyst) on the electrode, and the stirring speed (high speeds cause the catalyst to detach from the electrode). These considerations can cause the TN to vary by over a factor of 10.

Comparison of Quinone versus bpy in $[Ru_2(OH)_2(L)_2(btpyan)]^{2+}$ (L = Q, bpy). Wada et al. also carried out water oxidation by a related bipyridine complex $[Ru_2(OH)_2(bpy)_2(btpyan)]^{2+}$.[16] This complex displays metal-centered redox reactions at 0.79 V and an irreversible anodic wave at $E_p = 1.43$ V. The latter wave shifted to $E_p = 1.31$ V by the addition of water to the trifluoroethanol solution, indicating that $[Ru^{IV}(OH)(bpy)Ru^{IV}(OH)(bpy)]^{6+}$ is unstable and likely converts to $[Ru^{IV}(O)(bpy)Ru^{IV}(O)(bpy)]^{4+}$ by the loss of two protons (eq 12). Interestingly, unlike $[Ru^{II}(OH)(Q)Ru^{II}(OH)(Q)]^{2+}$, $[Ru^{II}(OH)(bpy)Ru^{II}(OH)(bpy)]^{2+}$ shows no dissociation of the hydroxo protons even in the presence of a large excess of *t*-BuOK.[16]

$$[Ru^{II}(OH)(bpy)Ru^{II}(OH)(bpy)]^{2+} \xrightarrow{-2e^-} [Ru^{III}(OH)(bpy)Ru^{III}(OH)(bpy)]^{4+} \xrightarrow{-2e^-} [Ru^{IV}(O)(bpy)Ru^{IV}(O)(bpy)]^{4+} + 2H^+ \quad (12)$$

A slight increase in irreversible currents at potentials of more than 1.5 V indicates that the oxidation product of $[Ru^{IV}(O)(bpy)Ru^{IV}(O)(bpy)]^{4+}$ has the capability of oxidizing water in trifluoroethanol/water, although the catalytic current is much smaller than that of the quinone analogue. While the CV of the ITO electrode modified with $[Ru^{II}(OH)(bpy)Ru^{II}(OH)(bpy)]^{2+}$ exhibited a small catalytic current at 1.70 V in H_2O (pH = 4.0), the amount of O_2 evolved by the controlled-potential electrolysis over a 5 h period was reported to be negligible compared to that of $[Ru^{II}(OH)(Q)Ru^{II}(OH)(Q)]^{2+}$.[16]

Computational Studies of Dinuclear Ru Catalysts: General Considerations. As previously discussed, the quinone ligands introduce additional redox couples into the catalyst, so that, in addition to the metal oxidation states (Ru^{II}, Ru^{III}, Ru^{IV}, etc.), there is the possibility of ligand redox states such as quinone, semiquinone, and catecholate. The absence of an oxo bridge in the Tanaka catalyst causes the total charge on the complex to be more positive than that, e.g., on the blue dimer catalyst, when the Ru oxidation states are the same. This might tend to destabilize the higher oxidation states of Ru in the Tanaka catalyst. For each of the possible intermediates along the catalytic reaction pathway, there are the usual complications of multiple spin states associated with several one-electron redox couples. The aim of the work presented here is to carry out theoretical studies to guide our experimental mechanistic investigations, making the initial iteration to explain what has been observed and to suggest ideas for future experimental studies.

Here we make a distinction between the "catalyst" and "reactant" parts of the catalyst/water moiety complex. The catalyst part, which it may not be possible to isolate experimentally, is assumed to begin the catalytic cycle in its most oxidized form, while water molecules (or perhaps

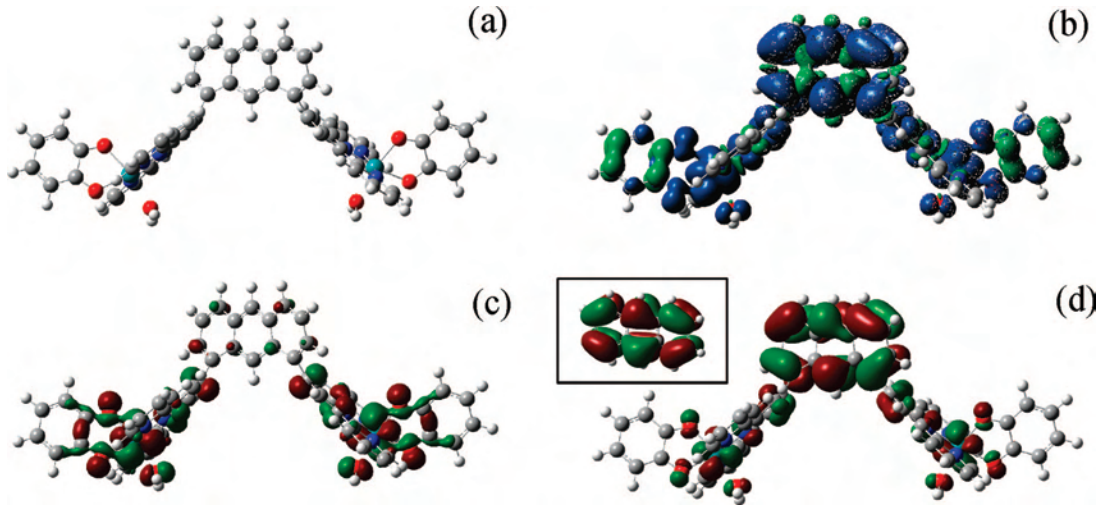

Figure 5. Computed geometrical and electronic properties of triplet and singlet $[Ru_2(OH_2)_2(Q)_2(btpyan)]^{6+}$: (a) the geometrical structure of the triplet state; (b) the spin density of the triplet state; (c) the HOMO of the singlet state; (d) the LUMO of the singlet state. The insert in part d shows the HOMO of anthracene.

OH^- ions), the most reduced form of oxygen, bind to vacant coordination sites on the catalyst. There are two possible types of electron-transfer reactions that can take place. The first is an "internal" electron transfer from a water moiety to the catalyst part of the complex. The second is from the catalyst/water moiety complex to the external world (e.g., at an electrode or to the medium). Here we focus on the possibility that the catalyst part can accommodate four internal electron transfers from the two bound water moieties, producing a species with an O−O bond, before it is necessary to oxidize the catalyst/water moiety complex by the transfer of four electrons to the external world as found experimentally above pH = 3.[16] These internal electron-transfer processes are triggered by the removal of protons from the complex to the external world through acid−base reactions.

The first question we address is, with what species do we associate the starting active form of the Tanaka catalyst (i.e., the form that binds water or hydroxide ions and is "fully" oxidized)? Perhaps naively, our initial notion was that $[(Ru^{III})_2(OH_2)_2(Q)_2(btpyan)]^{6+}$ might be a logical starting point because of the Ru^{III}/Ru^{II} and $Q/SQ^{\bullet -}$ couples providing four "holes", i.e., oxidized forms of one-electron redox couples. Based on the experimental pK_a results and spectroscopic data, our working model was that the catalyst must bind two water molecules from the solvent within close enough proximity to eventually form an O−O bond. Acid–base reactions with the solvent remove protons from the bound water molecules, and internal electron transfer occurs from the bound water moieties to the catalyst. At some point in this process, an O−O bond is formed and the catalyst is oxidized, but the order of proton transfers and catalyst oxidation is an open question. Release of O_2 from the oxidized catalyst and the binding of two more water molecules from the solvent complete the cycle.

Considering $[(Ru^{III})_2(OH_2)_2(Q)_2(btpyan)]^{6+}$, the most oxidized form of the catalyst (with two molecules of water) that may exist at low pH and a high applied potential, there is an unpaired spin on both Ru^{III} atoms so one would expect that the electronic ground state would be a triplet. Interestingly, the calculated spin density of the triplet state indicates that this electronic state does not really involve Ru^{III} but instead is the $(Ru^{+2.5})_2(btpyan^{\bullet +})^{6+}$ anthracene cation radical (Figure 5). Because this species would be unstable as a starting material, the corresponding singlet state was considered. The singlet state, which is calculated to lie 5.4 kcal/mol above the triplet state, places the last two electrons in a molecular orbital delocalized over both Ru centers. However, the lowest unoccupied molecular orbital (LUMO) of the singlet species is the HOMO of the anthracene moiety (Figure 5). This means that the proper assignment of the singlet 6+ complex is not $(Ru^{III})_2(btpyan)^{6+}$ but $(Ru^{II})_2(btpyan^{2+})^{6+}$. These results clearly indicate that the generation of anthracene cation radicals may be a recurring problem. A more promising candidate for the "most oxidized catalyst" species with coordinated H_2O would be $[(Ru^{II})_2(H_2O)_2(Q)_2(btpyan)]^{4+}$, i.e., the singlet 6+ species with two additional electrons to doubly occupy the anthracene HOMO. This result is a cautionary signal that one must be ever mindful of where the anthracene HOMO is lurking among the frontier orbitals. On the other hand, this consideration has the positive effect of eliminating many of the possible reaction pathways because they involve intermediates in which the anthracene HOMO is not doubly occupied.

Computational Studies of the $[(Ru^{II})_2(Q)_2(btpyan)]^{2+}$ Catalyst: An All-Singlet Pathway. Starting with $[(Ru^{II})_2(Q)_2(btpyan)]^{4+}$ (Figure 6a) as the catalyst part of the complex, a H_2O molecule or a hydroxide ion can be added to the vacant coordination position at each the two metal centers (Figure 6b,c). In the former case, two H_2O protons are very acidic and will readily dissociate to form the first of two singlet $[(Ru^{II})_2(OH)_2(Q)_2(btpyan)]^{2+}$ minima (denoted "far" owing to the large O−O distance of 4.6 Å). Our B3LYP calculations actually put the corresponding triplet state at the "far" singlet geometry 1.8 kcal/mol below this singlet state, but our CAS(4,4) calculations place the singlet state 4.1 kcal/mol below the triplet state at this geometry because of multiconfigurational effects. The two-electron oxidation of this singlet intermediate state results in a species that is

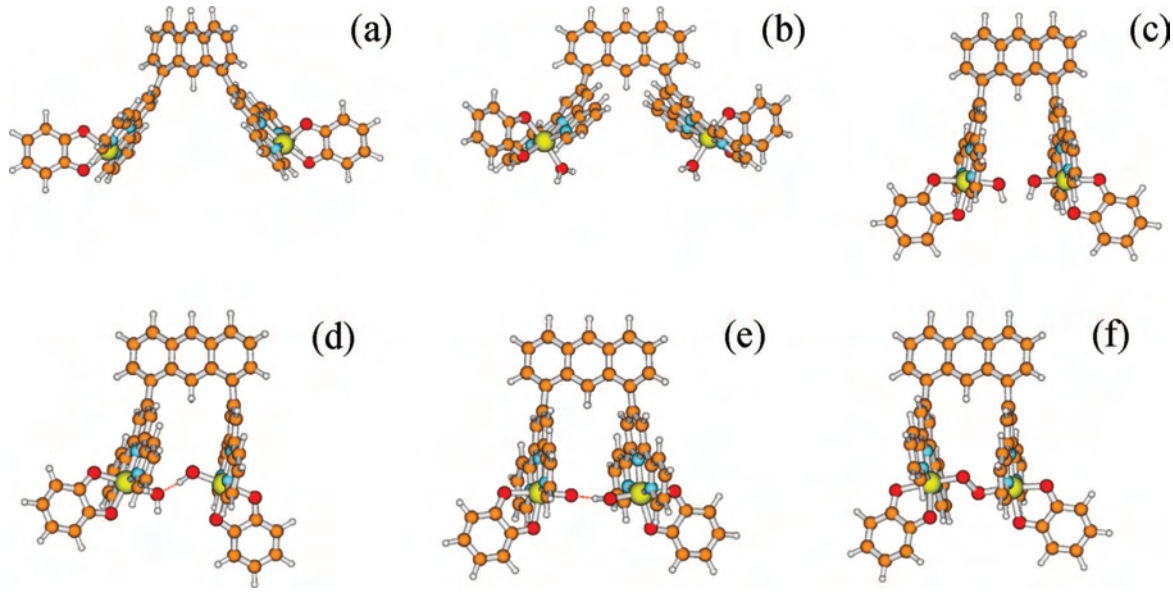

Figure 6. Relevant species along an all-singlet catalytic pathway for water oxidation starting with $[Ru_2(Q)_2(btpyan)]^{4+}$: (a) the bare catalyst; (b) the catalyst with two H_2O adducts; (c) the "far" dihydroxo adduct (see text); (d) the "near" dihydroxo adduct (see text) that is likely the species isolated and characterized by Tanaka's group; (e) the hydrogen-bonded species arising from deprotonation of part c or d; (f) the neutral O_2 adduct to the fully reduced form of part a.

unstable (for the same reason as $[Ru_2(OH_2)_2(Q)_2(btpyan)]^{6+}$) and that is unconnected to viable reaction intermediates. There is a second singlet $[(Ru^{II})_2(OH)_2(Q)_2(btpyan)]^{2+}$ minimum at a shorter (2.6 Å) O−O separation (denoted "near") that is 5.0 kcal/mol more stable than the "far" singlet (Figure 6d) and is asymmetrically hydrogen-bonded in a manner similar to the corresponding triplet-state minimum-energy structure (discussed below) that lies 13.5 kcal/mol below the "far" singlet minimum according to our B3LYP calculations. There is a transition state with a barrier of only 0.6 kcal/mol separating the "far" and "near" singlet minima. One of the two singlet minima must correspond to the species that was isolated and characterized by Tanaka's group,[16] and it is unlikely that the "far" minimum could be stable with a barrier to conversion to the "near" minimum comparable to k_BT, but the uncertainties in the B3LYP/LANL2DZ level of theory combined with the close separation and apparent crossing of the singlet and triplet potential energy surfaces in the vicinity of these singlet minima do not permit a detailed description of this singlet state at present. It could well be that the small-barrier transition state might disappear at a higher level of theory so that there would be only one singlet minimum. Continuing with the singlet pathway, as one of the acidic hydroxo protons is being extracted from $[(Ru^{II})_2(OH)_2(Q)_2(btpyan)]^{2+}$, the triplet surface becomes lower in energy and an intersystem crossing (ISC) is likely to occur to the triplet manifold of states. Because the triplet $[(Ru^{II})_2(OH)_2(Q)_2(btpyan)]^{2+}$ minimum lies 13.5 kcal/mol below the "far" singlet minimum and 8.5 kcal/mol below the "near" singlet minimum, it is clear that a seam of intersection between singlet and triplet energy surfaces exists near the minimum-energy geometry of this singlet state. The singlet $[(Ru^{II})_2(OH\cdots O)(Q)_2(btpyan)]^{+}$ species (Figure 6e) resulting from the loss of a proton from the $[(Ru^{II})_2(OH)_2(Q)_2(btpyan)]^{2+}$ species lies 15.1 kcal/mol above the corresponding triplet minimum, has a small O−O distance like the "near" singlet $[(Ru^{II})_2(OH)_2(Q)_2(btpyan)]^{2+}$, and has a strong hydrogen bond between the two bound O atoms that prevents the formation of an O−O bond (see Table 2). Removal of the hydrogen-bonded proton to the aqueous solution results in the formation of a neutral $[(Ru^{II})_2(O_2)(Q)_2(btpyan)]^{0}$ complex with an O−O bond (Figure 6f) that lies 8.2 kcal/mol above the corresponding triplet species. It is probably not worth exploring the 2+ and 4+ O_2-bonded singlet species generated by oxidation of the neutral complex because they are higher in energy than the corresponding triplet species. At any rate, in the singlet pathway, when the catalyst is regenerated in its original (singlet) form, spin conservation requires the liberation of $^1\Delta$ O_2 and not ground state $^3\Sigma^-$ O_2.

Computational Studies of the $[(Ru^{II})_2(Q)_2(btpyan)]^{2+}$ Catalyst: Crossing over to the Triplet Manifold. Now a pathway that crosses over to the triplet manifold of states during the catalytic cycle will be considered. The first step is the same as that in the singlet mechanism: the experimentally observed singlet intermediate is formed. Then as a proton is pulled into the solution or even if there is a significant distortion in the geometry of the singlet intermediate, the system crosses over to the triplet potential energy surface and falls either into the 2+ triplet species $[Ru_2(OH\cdots OH)(Q)_2(btpyan)]^{2+}$ (Figure 7a) that has a much shorter O−O distance than the "far" singlet $[(Ru^{II})_2(OH)_2(Q)_2(btpyan)]^{2+}$ and is hydrogen-bonded in an asymmetric fashion (i.e., the two OH^- groups are not equivalent) or the 1+ triplet species $[Ru_2(OH\cdots O)(Q)_2(btpyan)]^{+}$ (Figure 7b), which is similar in structure to the 1+ singlet but more stable. The proton of the 2+ triplet that is not involved in the hydrogen bond is more acidic and should be readily removed to form the 1+ triplet $[Ru_2(OH\cdots O)(Q)_2(btpyan)]^{+}$ if the latter species is not formed directly from the "near" singlet $[(Ru^{II})_2(OH)_2(Q)_2(btpyan)]^{2+}$. Based on atomic spin densities, this 1+ triplet species has semiquinone ligands. It should

Table 2. Calculated Bond Distances (Å) of Key Intermediates along the Water Oxidation Pathway[a]

	$^1[Ru_2(OH_2)_2(Q)_2]^{4+}$	"far" $^1[Ru_2(OH)_2(Q)_2]^{2+}$	"near" $^1[Ru_2(OH)_2(Q)_2]^{2+}$	$^3[Ru_2(OH)_2(Q)_2]^{2+}$	$^3[Ru_2(OH\cdots O)(Q)_2]^{+}$	$^3[Ru_2(O_2)(Q)_2]^{0}$	$^3[Ru_2(O_2)(Q)_2]^{2+}$	$^3[Ru_2(O_2)(Q)_2]^{4+}$
Ru−O (H_2O moiety)	2.148	1.981	2.003	1.986	1.851	2.011	2.030	2.037
	2.148	1.981	1.954	1.943	1.950	1.993	2.030	2.051
Ru−O1	2.022	2.015	2.017	2.042	2.100	2.086	2.079	2.077
	2.022	2.015	2.017	2.094	2.106	2.075	2.079	2.075
Ru−O2 (quinones)	2.071	2.110	2.119	2.117	2.101	2.105	2.092	2.099
	2.071	2.110	2.102	2.092	2.116	2.113	2.092	2.092
C1−O1	1.315	1.329	1.333	1.337	1.349	1.349	1.321	1.301
	1.314	1.329	1.326	1.337	1.333	1.354	1.321	1.302
C2−O2 (quinones)	1.312	1.325	1.329	1.329	1.348	1.345	1.322	1.302
	1.312	1.325	1.322	1.341	1.333	1.349	1.322	1.303
C3−C4	1.384	1.390	1.392	1.389	1.399	1.401	1.388	1.381
	1.384	1.390	1.388	1.393	1.393	1.403	1.388	1.382
C5−C6	1.384	1.388	1.392	1.391	1.399	1.402	1.388	1.381
	1.384	1.388	1.387	1.393	1.393	1.404	1.388	1.381
C4−C5 (quinones)	1.458	1.442	1.439	1.441	1.426	1.424	1.444	1.463
	1.458	1.442	1.444	1.435	1.434	1.421	1.444	1.463
O−O	9.945	4.550	2.628	2.666	2.652	1.461	1.403	1.400
∠Ru−C−Ru (deg)	79.5	42.6	35.4	35.3	34.1	29.7	30.3	30.1

[a] Here species are identified by their composition, total charge, and spin multiplicity without explicit assignment of metal or ligand oxidation states. More detailed assignments are discussed in the text.

Figure 7. Intermediates along the triplet portion of the catalytic pathway for water oxidation by $[Ru_2(Q)_2(btpyan)]^{4+}$: (a) the hydrogen-bonded dihydroxo adduct; (b) the hydrogen-bonded species resulting from the deprotonation of part a; (c) the fully reduced neutral O_2 adduct; (d) the partially oxidized 2+ O_2 adduct.

be more difficult to remove the remaining hydrogen-bonded proton to reach the neutral triplet species, $[Ru_2(O_2)(Q)_2(btpyan)]^0$ (Figure 7c) in which an O−O bond is formed. In this species, the ligands are somewhere between semiquinones and catecholates based on atomic spin densities. If it were not for the O_2 moiety attracting a significant negative charge, they would probably be catecholates, and the near constancy of the C−C bonds in the quinone ligand (see Table 2) is consistent with the catecholate assignment. If we revert to integer formal charges (rather than the fractional ones based on spin densities), we can view these crucial two deprotonation steps as both being proton-coupled two-electron-intramolecular-transfer reactions involving the water moieties and the two quinone ligands:

$$[(Q)Ru^{II}-(OH\cdots OH)^{2-}-Ru^{II}(Q)]^{2+} \rightarrow [(SQ)Ru^{II}-(OH\cdots O)-Ru^{II}(SQ)]^{+}+H^{+}$$

$$[(SQ)Ru^{II}-(OH\cdots O)^{-}-Ru^{II}(SQ)]^{+} \rightarrow [(Cat)Ru^{II}-(O_2)-Ru^{II}(Cat)]^{0}+H^{+}$$

These two steps achieve complete separation of the charges involved in the redox reaction: the protons go into solution and the electrons go onto the quinone ligands of the catalyst. The experimental results indicate that the rest potential of the neutral species is ~0 V and this species has an absorption band at 850 nm, consistent with the assignment of incomplete two-electron transfer (based on the spin density) accompanying the removal of the second proton and suggesting a species with quinone ligands intermediate between semiquinone and catecholate. It is striking that this neutral species corresponds to the fully reduced form of the catalyst (i.e., any oxidation of the starting complex, $[Ru_2(OH)_2(Q)_2(btpyan)]^{2+}$ or $[Ru_2(OH_2)_2(Q)_2(btpyan)]^{4+}$, by transfer of electrons to the external world has not taken place at this stage).

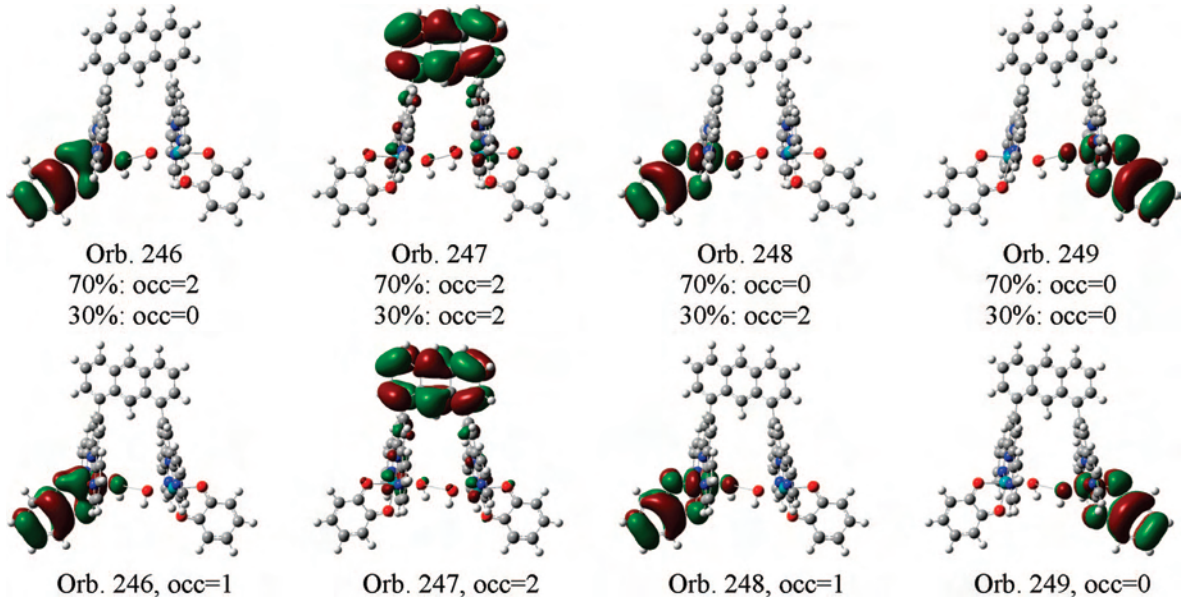

Figure 8. Active space orbitals and occupations from CAS(4,4) calculations of singlet (top) and triplet (bottom) $[Ru_2(OH)_2(Q)_2(btpyan)]^{2+}$.

It is not clear whether the oxidation of the neutral complex should occur in sequential one-electron steps, two two-electron steps, or a single four-electron step, but the CV studies in CF_3CH_2OH/ether indicated that the formation of $[Ru_2(O_2)(Q)_2(btpyan)]^{+}$ and $[Ru_2(O_2)(Q)_2(btpyan)]^{2+}$ occurs by sequential one-electron-oxidation steps at $E_p = 0.30$ and 0.40 V, respectively. The species formed after the electrolysis of $[Ru_2(O_2)(Q)_2(btpyan)]^{0}$ at 0.55 V showed a band at 582 nm, indicating a quinone nature. A final two-electron step (or sequential one-electron steps) having an irreversible anodic wave was observed at $E_p = 1.34$ V based on the area of the broad anodic wave.[16] Upon the addition of 10% H_2O to the solution, strong catalytic currents at potentials more positive than +1.0 V were observed. Our calculations indicate that the removal of the first two electrons produces $[Ru_2(O_2^{-})(Q^{-0.5})_2(btpyan)]^{2+}$ (Figure 7d) that has ligands intermediate between quinone and semiquinone, again because the O_2 moiety attracts some of the negative charge that would otherwise provide more semiquinone character. The last two-electron oxidation step that liberates O_2 in the ground $^3\Sigma^-$ state and regenerates the oxidized form of the catalyst via the production of $[Ru_2(O_2)(Q)_2(btpyan)]^{4+}$ is more problematic, as will be discussed below. Other triplet species were considered, e.g., $[Ru_2(OH)_2(Q)_2(btpyan)]^{4+}$ and $Ru_2(OH\cdots O)(Q)_2(btpyan)]^{3+}$, the two-electron-oxidized forms of $[Ru_2(OH)_2(Q)_2(btpyan)]^{2+}$ and $Ru_2(OH\cdots O)Q)_2$-$(btpyan)]^{+}$, respectively, but they also exhibited anthracene cation radical behavior and were significantly spin-contaminated.

Returning now to the issue of the relative stability of the singlet and triplet $[Ru_2(OH)_2(Q)_2(btpyan)]^{2+}$ at the optimized geometry of the "far" singlet, our CAS(4,4) calculations indicate that the singlet has two important configurations. The triplet has only one important configuration. As mentioned above, the CAS(4,4) results place the singlet state 4.1 kcal/mol below the triplet. The active space orbitals are quite similar for the two states, and the important configurations are closely related. In the singlet state, there is a pair of electrons shared 70% and 30%, respectively, between a bonding π orbital involving one of the Ru centers and its quinone ligand, and the corresponding antibonding π orbital. This is a typical generalized valence-bond type of CI, which generates some open-shell singlet character upon the projection of the molecular orbitals onto fragment orbitals (i.e., Ru^{III}-semiquinone character). The CAS(4,4) calculation performs a valence CI involving the occupied orbitals containing the four highest-energy electrons and the one or two of the lowest unoccupied molecular orbitals necessary to make a total of four orbitals in the active space. For the singlet, this is the HOMO−1 HOMO, LUMO, and LUMO+1. For the triplet, it is the HOMO−2, HOMO−1, HOMO, and LUMO, but it is the same set of orbitals in both cases. The quoted percentages refer to the percentage of the full CAS wave function contributed by a given orbital configuration (i.e., set of orbital occupancies) as determined by the square of its coefficient in the CI expansion. As is seen in Figure 8, the orbital that corresponds to the anthracene HOMO (and that is the HOMO in the principal configuration of the singlet complex) is doubly occupied in both important singlet configurations. In the triplet, the orbital corresponding to the anthracene HOMO is also doubly occupied, and instead of sharing a pair of electrons as in the GVB-type CI of the singlet, there is a single electron in both bonding and antibonding Ru−Q π orbitals.

Finally, we turn to the problematic nature of triplet $[(Ru)_2(O_2)(Q)_2(btpyan)]^{4+}$ as a possible intermediate. Its structure is shown at the left in Figure 9, while its spin density is displayed on the right. Because the O_2 moiety attracts substantial negative charge, stabilized by the two Ru centers that sandwich it, the orbital corresponding to the anthracene HOMO is electron-deficient. Based on Mulliken atomic spin densities and charges, the anthracene moiety has an excess α spin of 1.00 electron and a charge of +0.99, allowing the assignment of the redox state of this species as $[(Ru^{II})_2(O_2)(Q)_2(btpyan^{\bullet+})]^{4+}$. The corresponding singlet state

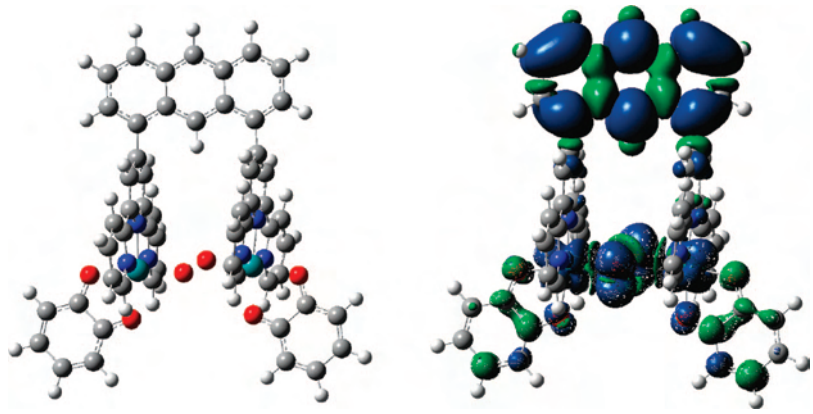

Figure 9. Calculated geometrical structure and spin density of triplet $[Ru_2(O_2)(Q)_2(btpyan)]^{4+}$.

is 10.7 kcal/mol higher in energy than this triplet anthracene cation radical, which should be very unstable. It is therefore questionable whether this species is involved in the catalytic cycle. Certainly, a more detailed energetic and mechanistic investigation is needed. It is interesting to point out that the formation of this species takes place at $E_p = 1.34$ V; however, O_2 production takes place above 1.60 V.[16] This fact may be associated with the overpotential required to obtain a catalytic current from the observed $[(Ru)_2(O_2^-)(Q^{-0.5})_2(btpyan)]^{2+}$ intermediate. The overpotential may be associated with the need to remove the electron from the O_2^- moiety (as well as the electron on the quinones), causing repulsion of the Ru^{II} centers and liberation of O_2 without forming $[(Ru^{II})_2(O_2^-)(Q)_2(btpyan^{\bullet+})]^{4+}$. The requirement of such an overpotential may also be due to the relatively large resistance between the ITO electrode and the physically attached catalysts.

The two unpaired electrons in the calculated triplet $[(Ru^{II})_2(O_2^-)(Q)_2(btpyan^{\bullet+})]^{4+}$ species reside on the O_2 and anthracene moieties. If Ru^{III} is involved in the catalytic cycle at all, it would most likely be in this final stage, but our calculations tell us that the removal of two electrons from the triplet $[(Ru)_2(O_2^-)(Q)_2(btpyan)]^{2+}$ species would come from the SQ/Q and anthracene moieties and not the metal centers.

Proposed Catalytic Reaction Pathway for the $[(Ru^{II})_2(Q)_2(btpyan)]^{2+}$ Catalyst. The diagram in Figure 10 summarizes what we have learned or think we have learned so far about the catalytic pathway for water oxidation with Tanaka's catalyst. It shows the calculated structures, indicates the O−O separation and the Ru−C−Ru angle (where C is the carbon atom at the top of the middle anthracene ring), and assigns the redox states of each species along the proposed reaction path. Selected bond distances and angles of these species are summarized in Table 2. As we mentioned before, the bond distances such as C−O and C−C (of the quinone ligand) depend on the nature of the electronic structure of the quinone ligand (i.e., longer and shorter C−O distances for the catecholate and quinone ligands, respectively; relatively similar C−C distances of the phenyl ring for the catecholate ligand). Our calculated distances for the Tanaka catalyst and its intermediates show the expected trends for the assignments given.

The O−O separation becomes shorter once the system has reached the "near" singlet dihydroxo species or crossed to the triplet manifold and then shorter again once the last proton is removed and an O−O bond is formed. It seems unlikely that the reaction of $[Ru_2(O_2)(Q)_2(btpyan)]^{4+}$ to liberate O_2 would occur without the involvement of either H_2O molecules or OH^- ions to displace the O_2. There might be an oxidation route that bypasses this species to produce the $[Ru_2(OH)_2(Q)_2(btpyan)]^{2+}$ species and O_2 from the two-electron-oxidized species $[Ru_2(O_2)(Q)_2(btpyan)]^{2+}$. There is also a possibility of both solvent and electronic effects not considered here (e.g., replacing *t*-Bu groups on quinone by H) affecting the computed ligand properties and energetics of the various species.

The striking features of the scheme shown here are (1) that the Ru centers remain predominantly in their 2+ formal oxidation state (i.e., as the predominant component in often intermediate cases between 2+ and 3+) throughout the entire catalytic cycle and (2) that all of the redox reactions involve only the coordinated water moieties and the quinone ligands. This mechanism is entirely different from those proposed for μ-oxoruthenium dinuclear complexes. The absence of a μ-oxo bridge in the Tanaka catalyst causes the destabilization of the higher oxidation states of Ru. However, water oxidation catalysts containing a Ru^{II} dinuclear species without a μ-oxo bridge have been investigated[43,46] and the involvement of $Ru^{IV}-Ru^{IV}$ is proposed in some cases.[43] The Tanaka catalyst has H_2O or OH^- bound to Ru^{II} centers, and subsequent intramolecular electron-transfer reactions coupled with H^+ removal from the water moiety can only reduce the quinone ligands of the catalyst. The role of $[(Ru^{II})_2(O_2^-)(Q^{-1.5})_2(btpyan)]^0$, which is formed by removal of all four protons before four-electron oxidation takes place, as the most reduced catalyst species is noteworthy. The role of the Ru^{II} centers appears to be that they mediate the intramolecular electron transfer from the water moieties to the quinone ligands because their d orbitals overlap appropriately with both species. For example, inspection of Figure 8 shows that orbitals 246 and 248 are delocalized over the quinone moiety, the Ru center, and the OH^- on

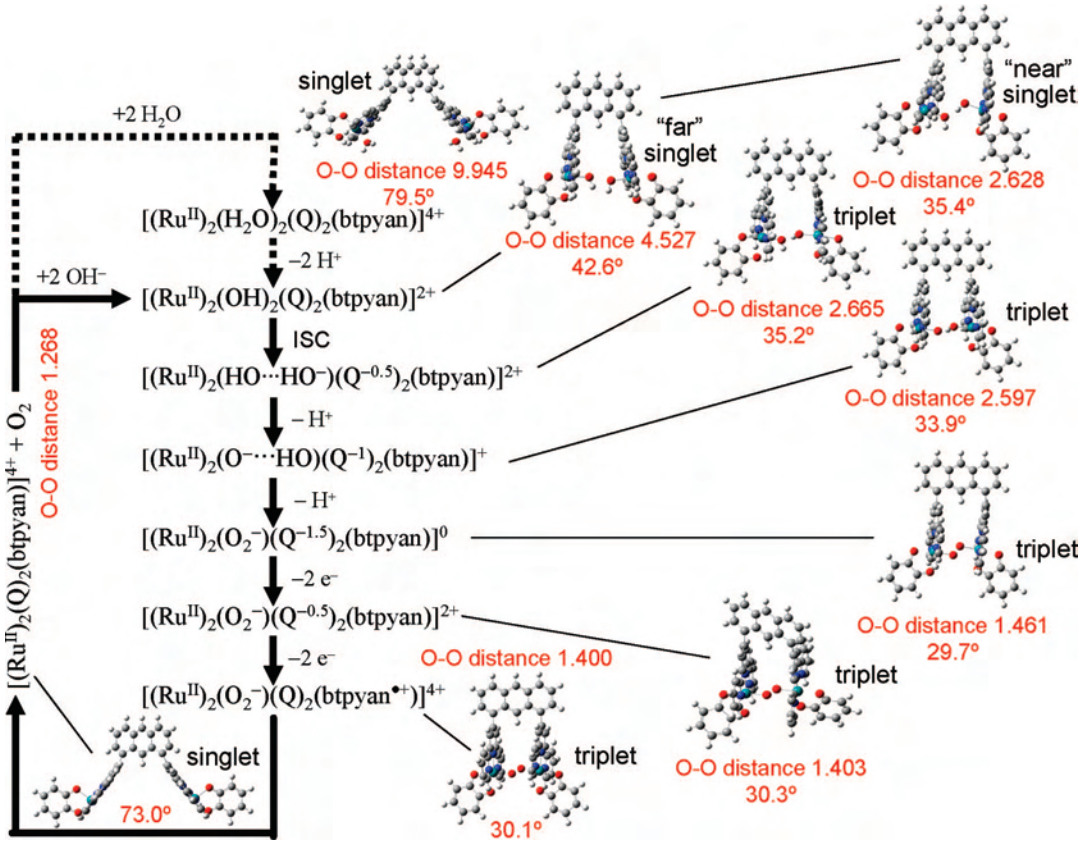

Figure 10. Proposed catalytic pathway for H_2O oxidation by $[Ru_2(Q)(btpyan)]^{4+}$, the oxidized form of the catalyst. Listed for each species is the O−O distance and the Ru−C−Ru angle, where the C atom is at the top center of the anthracene moiety. First, two water molecules or two hydroxide ions bind to vacant coordination sites to form the "far" singlet dihydroxo species with an O−O distance of 4.527 Å. This species has a barrier comparable to k_BT to form the "near" singlet, hydrogen-bonded species of the same composition. This "near" singlet species is likely the species isolated and characterized by Tanaka's group. Upon geometric distortion of this species along a proton dissociation coordinate, the system likely crosses over to a triplet manifold for the remainder of the catalytic cycle. All of the triplet species shown are considerably more stable than the corresponding singlets. It is likely that all four protons are removed before the catalyst/water moiety complex is externally oxidized (see text). Accompanying proton removal, electron transfer occurs from the bound water moieties to the quinone ligands as indicated. The involvement of the final 4+ O_2-bound intermediate is unlikely.

one side of the complex. Orbital 249 is delocalized in a similar manner on the other side of the complex.

While our gas-phase calculations predict that the $[(Ru^{II})_2(O_2{}^{-1.5})(Q)_2(btpyan^{\bullet+})]^{4+}$ intermediate is produced by $4e^-$ oxidation of $[(Ru^{II})_2(O_2{}^-)(Q^-)_2(btpyan)]^0$, we believe we need to carry out calculations with some explicit water molecules and a polarizable continuum model of a bulk aqueous solution in order to confirm the robustness of this result. Such calculations, which will also permit a more reliable description of the energetics along the sequence of proposed intermediates, are underway.

Comparison of Chemical Properties of Xanthene-Bridged Dinuclear Ru Species vs Anthracene-Bridged Dinuclear Ru Species. The water oxidation catalyst complex $[Ru_2(OH)_2(Q)_2(btpyan)]^{2+}$ has a rather rigid framework owing to the sterically fixed, planar anthracene bridge. Does a more flexible bridge provide a better opportunity for the formation of a Ru−O−O−Ru species? To explore this question, a ruthenium complex with a bridging btpyxa [2,7-di-*tert*-butyl-9,9-dimethyl-4,5- bis(2,2′:6′,2″-terpyrid-4′-yl)-xanthene] ligand was prepared (see Scheme 2).[88] While the two terpyridine units bridged by either a xanthene or a anthracene moiety (in btpyxa or btpyan, respectively) are

Scheme 2. Structures of btpyxa and $[(Ru)_2(\mu\text{-}O)(Q)_2(btpyxa)]^{3+}$

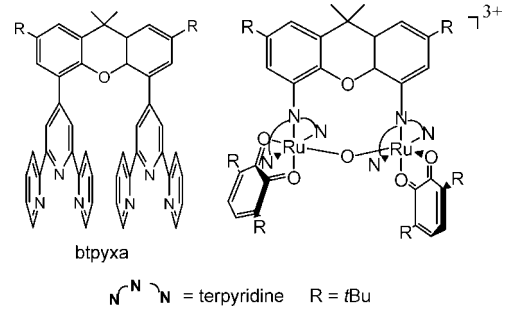

not able to rotate freely because of their steric repulsion, the sp^3 C and O atoms provide some additional flexibility in the xanthene-bridged complex. The UV–vis spectrum of $[Ru_2(Cl)_2(Q)_2(btpyxa)]^{2+}$ in CH_2Cl_2 shows a strong band at 598 nm. While this complex was originally assigned as $[(Ru^{III})_2(Cl)_2(SQ)_2(btpyxa)]^{2+}$,[88] the assignment of $[(Ru^{II})_2(Cl)_2(Q)_2(btpyxa)]^{2+}$ seems more consistent with the rest potential at 0.26 V. Furthermore, the spectral changes of λ_{max} 598 nm → 882 nm → 866 nm → a weak band at ~580 nm and a shoulder at ~450 nm during reduction from 0.20 to −0.90 V may correspond to the change from $[(Ru^{II})_2(Cl)_2(Q)_2(btpyxa)]^{2+} \rightarrow [(Ru^{II})_2(Cl)_2(Q)(SQ)(btpyxa)]^{+} \rightarrow [(Ru^{II})_2(Cl)_2(SQ)_2(btpyxa)]^0 \rightarrow [(Ru^{II})_2(Cl)_2(Cat)_2(btpyxa)]^{2-}$. A

(88) Wada, T.; Tanaka, K. *Eur. J. Inorg. Chem.* **2005**, 3832–3839.

detailed investigation of the electronic structures may be needed. In $[(Ru^{II})_2(Cl)_2(Q)_2(btpyxa)]^{2+}$, the coordinating Cl ligand cannot be replaced by water or a hydroxide ion. Is $[(Ru^{II})_2(Cl)_2(Q)_2(btpyxa)]^{2+}$ a water oxidation catalyst like Thummel's Cl-bridged Ru dinuclear species,[46] even though the complex has coordinating Cl ligands? While water oxidation using Ce^{IV}/H^+ or other sacrificial oxidants has not been investigated, a preliminary result indicates that no O_2 evolution takes place in the controlled electrolysis of $[(Ru^{II})_2(Cl)_2(Q)_2(btpyxa)]^{2+}$ in CF_3CH_2OH/EtOEt (1:1, v/v) in the presence of H_2O (10%) at 1.70 V.

An oxo-bridged diruthenium species $[(Ru^{III})(Ru^{IV})(\mu\text{-}O)(SQ)_2(btpyxa)]^{3+}$ (or $[(Ru^{II})(Ru^{III})(\mu\text{-}O)(Q)_2(btpyxa)]^{3+}$) has been identified in the reaction of $[Ru_2Cl_6(btpyxa)]^0$ with 3,6-di-*tert*-butylcatecholate in MeOH with *t*-BuOK.[88] While the electrochemical and spectroscopic properties of this μ-oxo species and its mono- and direduced species have been investigated only to a limited extent, this system appears to offer many opportunities for the investigation of the electronic structures of the various intermediates (i.e., metal oxidation state, Q vs SQ, etc.). However, when we consider the effectiveness of such a species as a water oxidation catalyst, significant steric hindrance may need to be incorporated in the btpyxa ligand to suppress the deleterious Ru−O−Ru formation and allow the desired Ru−O−O−Ru formation.

Substituent Effects of Quinone Ligands on the Catalytic Activity. Experimental and theoretical evaluation of the charge distribution over the ruthenium and quinone framework has been published for a series of $[Ru^{II}(OAc)(SQ)(tpy)]$ complexes having various substituents on the semiquinone ligand (SQ = 3,5-*t*-Bu_2SQ, 4-*t*-BuSQ, 4-ClSQ, 3,5-Cl_2SQ, and Cl_4SQ).[89] While the Q/SQ and SQ/Cat potentials shift more negative with the order of the substituents listed, the rest potentials are always between the Q/SQ and SQ/Cat potentials, indicating Ru^{II}-semiquinone frameworks. These complexes all have an absorption band at ~890 nm; however, the intensities decrease with the order of the substituents above. Furthermore, EPR and DFT calculations demonstrated successive changes of the electronic structure of the Ru-semiquinone framework in which the Ru^{III}-catecholate contribution increases with an increase in the electron-withdrawing character of the substituents on the semiquinone ligands.

Does an electron-withdrawing group on the quinone enhance the catalytic acitivity for water oxidation? We have recently prepared $[(Ru^{II})_2(OH)_2(SQ)_2(btpyan)]^0$ [where SQ is 3,6-(*t*-$Bu)_2$Q, 3,5-Cl_2SQ, or 4-(NO_2)SQ].[90] When SQ is 3,6-(*t*-$Bu)_2$SQ, the species is the two-electron-reduced species of the isolated Tanaka catalyst, $[(Ru^{II})_2(OH)_2(Q)_2(btpyan)]^{2+}$. Preliminary CV results in water (pH = 4.0) using an ITO electrode modified with $[(Ru^{II})_2(OH)_2(SQ)_2(btpyan)]^0$ [SQ = 3,5-Cl_2SQ or 4-(NO_2)SQ] indicate that the Cl- and NO_2-substituted complexes do not show any catalytic activity upon application of up to 2.0 V vs Ag/AgCl. This result is in sharp contrast to that with the *t*-Bu_2-substituted complex. The $[(Ru^{II})_2(OH)_2(SQ)_2(btpyan)]^0$ complex with SQ = 3,5-Cl_2SQ was oxidized to $[(Ru^{II})_2(OH)_2(Q)_2(btpyan)]^{2+}$ by excess Ce^{IV} (dissolved in CH_3CN) so that it is of interest to explore a pathway analogous to that proposed for the *t*-Bu_2-substituted complex. Because the electron-withdrawing groups shift all potentials, including the Q/SQ and SQ/Cat potentials, to more positive values, as well as affect the relative electronegativities of the ligands, the catalyst may not behave in the same way. Indeed, preliminary results suggest that the second deprotonation step leading to O−O bond formation does not occur.[87] Another possibility is that the applied potential of 2.0 V may not be sufficient for the two-electron oxidation of $[(Ru^{II})_2(O_2^-)(Q^{-0.5})_2(btpyan)]^{2+}$. A delicate balance of the charge distribution over the Q−Ru−OH framework may control the catalytic activity for water oxidation. More detailed results will be published elsewhere.[87]

Conclusions

We can draw several conclusions about the mechanism of water oxidation with Tanaka's catalyst. First, the proposed mechanism is *consistent with experimental observations*. After formation of the experimentally isolated singlet species, $[Ru_2(OH)_2(Q)_2(btpyan)]^{2+}$, an *ISC takes the complex into a triplet manifold* for the rest of the catalytic cycle. It is most likely that *all protons are removed to form the catecholate species, $[Ru_2(O_2^-)(Q^{-1.5})_2(btpyan)]^0$, before the complex is oxidized*. Surprisingly, unlike other reported Ru dinuclear water oxidation catalysts including the well-characterized blue dimer, the *predominant formal oxidation state of the two Ru atoms remains unchanged at 2+* during the entire catalytic cycle according to our gas-phase calculations. Instead of an effective charge neutralization by a sequence of proton removals and one-electron oxidations (i.e., $[(bpy)_2(OH_2)Ru^{III}ORu^{III}(OH_2)(bpy)_2]^{4+} \rightarrow [(bpy)_2(OH)Ru^{IV}ORu^{III}(OH_2)(bpy)_2]^{4+}$, etc.),[14,20,48,50] the removal of protons from $[(Ru^{II})_2(OH)_2(Q)_2(btpyan)]^{2+}$ takes place with a change in the total charge to form $[Ru_2(O_2^-)(Q^{-1.5})_2(btpyan)]^0$. Here the *active redox couples are SQ/Q and Cat/SQ* (consistent with the analogous complex with bpy ligands being inactive under similar conditions). While the two-electron oxidation of this species occurs at a moderate 0.4 V, the troublesome step is the next oxidation. Because it is not a proton-coupled electron-transfer reaction, the application of a relatively high potential (1.34 V vs Ag/AgCl) is needed to form $[(Ru^{II})_2(O_2^-)(Q)_2(btpyan^{\bullet+})]^{4+}$. It is clear that $Ru(bpy)_3^{3+}$, a frequently used sacrificial oxidant, cannot efficiently oxidize this species. However, this catalyst immobilized on an ITO electrode is very stable and produces a large amount of O_2 without decomposition. This may be due to the charge stabilization/distribution in the catalyst through a site-to-site interaction between metal, quinone, and the coordinated water moiety.

The theoretical work presented here represents the simplest approach, and the actual case is likely to be much more

(89) Wada, T.; Yamanaka, M.; Fujihara, T.; Miyazato, Y.; Tanaka, K. *Inorg. Chem.* **2006**, *45*, 8887–8894.

(90) Wada, T.; Tsai, M.-K.; Muckerman, J. T.; Fujita, E.; Tanaka, K.,to be published.

(91) Raven, S. J.; Meyer, T. J. *Inorg. Chem.* **1988**, *27*, 4478–4483.

complicated, although we are confident that the predominant Ru oxidation state must remain 2+ owing to the formation of the anthracene cation radical under electron-deficient conditions. It has been over 25 years since the discovery of the blue dimer as a water oxidation catalyst, and there is still controversy about the mechanism of the formation of O_2 in the final stage of the blue dimer mechanism.[22,23,48,51,54,91] Theoretical and experimental mechanistic studies with the Tanaka catalyst have just been initiated, and many questions remain to be answered. While we need to repeat and extend some of our previous experiments, we need many more new theoretical and experimental studies to fully understand this system and other related systems containing quinone derivatives.

In future theoretical work, we will include the explicit treatment of H_2O solvent molecules hydrogen-bonded to accessible oxygen sites and include both an explicit and a polarizable continuum model treatment of the H_2O solvent. Transition states and the energetics of proton- and electron-transfer steps will also be addressed. On the experimental side, we have initiated the preparation of the catalyst with a functionalized top of the anthracene ring for chemical attachment to electrodes. This will allow us to carry out spectroelectrochemistry and cyclic voltammetry on the dinuclear catalyst to identify the proposed intermediates.

Acknowledgment. The work at Brookhaven National Laboratory is funded under Contract DE-AC02-98CH10886 with the U.S. Department of Energy and supported by its Division of Chemical Sciences, Geosciences, & Biosciences, Office of Basic Energy Sciences.

Supporting Information Available: TD-B3LYP-calculated $Ru^{II}(OH_2)(Q)^{2+}$ spectrum (Figure S1), TD-B3LYP-calculated $Ru^{II}(OH)(Q)^{+}$ (singlet) and $Ru^{III}(OH)(SQ)^{+}$ (triplet) spectra (Figure S2), and optimized Cartesian coordinates of various dimeric Ru complexes. This material is available free of charge via the Internet at http://pubs.acs.org.

IC701892V